HHS Public Access

Author manuscript

Neuron. Author manuscript; available in PMC 2025 January 17.

Published in final edited form as:

Neuron. 2024 January 17; 112(2): 247–263.e6. doi:10.1016/j.neuron.2023.10.008.

The bone transcription factor Osterix controls extracellular matrix and node of Ranvier related gene expression in oligodendrocytes

Benayahu Elbaz[1,*], **Alaa Darwish**[2], **Maia Vardy**[1], **Sara Isaac**[2], **Haley Margaret Tokars**[1], **Yulia Dzhashiashvili**[1], **Kirill Korshunov**[3], **Murali Prakriya**[3], **Amir Eden**[2], **Brian Popko**[1,4,*]

[1]Department of Neurology, Division of Multiple Sclerosis and Neuroimmunology, Feinberg School of Medicine, Northwestern University, Chicago, Illinois

[2]Department of Genetics, The Alexander Silberman Institute of Life Sciences, The Hebrew University of Jerusalem, Jerusalem, Israel

[3]Department of Pharmacology, Feinberg School of Medicine, Northwestern University, Chicago, Illinois

[4]Lead contact

Summary

Oligodendrocytes are the primary producers of many extracellular matrix (ECM) related proteins found in the CNS. Thereby, oligodendrocytes play a critical role in the determination of brain stiffness, node of Ranvier formation, perinodal ECM deposition and perineuronal net formation, all of which depend on the ECM. Nevertheless, the transcription factors that control ECM related gene expression in oligodendrocytes remain unknown. Here, we found that the transcription factor Osterix (also known as Sp7) binds in proximity to genes important for CNS ECM and node of Ranvier formation and mediates their expression. Oligodendrocyte-specific ablation of *Sp7* changes ECM composition and brain stiffness, and results in aberrant node of Ranvier formation. Sp7 is known to control osteoblast maturation and bone formation. Our comparative analyses suggests that Sp7 plays a conserved biological role in oligodendrocytes and in bone forming cells, where it mediates brain and bone tissue stiffness by controlling expression of ECM components.

Graphical Abstract

[*]Correspondence: benayahu.elbaz-eilon@northwestern.edu, brian.popko@northwestern.edu.

Author contributions

B.E. and B.P. designed the study. B.E. injected the animals, harvested the tissues, cultured the primary oligodendrocytes and performed the ATAC-seq experiment, the bulk RNA-seq experiment and TEM analysis. M.A. and H.A. performed the IHC experiments and analyzed data. MP and KR isolated and cultured the Primary hippocampal neurons. Y.D. performed the RNAscope experiment. A.D. and S.I. performed the ChIP-seq experiments and analyzed the RNA-seq, ATAC-seq and the ChiP-seq experiments. A.E. designed and analyzed the RNA-seq, ATAC-seq and the ChiP-seq experiments. B.E. and B.P. wrote the manuscript, with input from all authors.

Declaration of interests

The authors declare no competing interests.

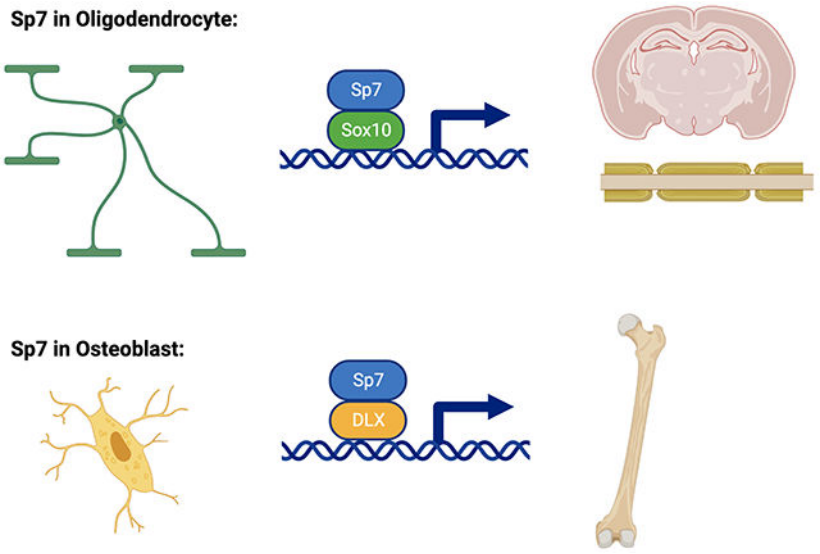

eTOC Blurb

Elbaz et al. show that Sp7 mediates the expression of genes required for node of Ranvier and brain ECM formation in mature oligodendrocytes. Moreover, Elbaz et al., show that Sp7 regulates ECM gene expression in a similar manner in oligodendrocytes and osteoblasts.

Introduction

Myelin is a multilayered lipid membrane structure that ensheathes and insulates axons, allowing for efficient propagation of action potentials. In the CNS, myelin is produced by oligodendrocytes[1]. Besides myelin synthesis, oligodendrocyte lineage cells are the sole or main producers of many extracellular matrix (ECM) related proteins[2-7]. By producing ECM proteins, oligodendrocytes are involved in node of Ranvier formation[8-10], in perinodal ECM formation[11] and in the formation of perineuronal nets (PNN)[4]. While the transcriptional control of myelin related gene expression in oligodendrocytes has been extensively studied[12-14], the regulation of ECM related genes in oligodendrocytes is largely unknown.

Brain ECM is compartmentalized into distinct structures at perineuronal nets around certain neurons, at axonal initial segment, around synapses, and at perinodal ECM that engulf the nodes of Ranvier. Perinodal ECM appears as myelination is completed, and acts as an ion-diffusion barrier that affects axonal conduction speed[11,15-18]. Brain ECM is primarily composed of hyaluronic acid, structural proteins, proteoglycans, glycoproteins, matricellular proteins and other molecules[16]. The composition and physical properties of brain ECM are constantly modified during normal development and aging, and under pathological conditions, such as demyelination and remyelination.

The zinc-finger protein Sp7 (also known as Osterix) is specifically expressed by mature oligodendrocytes in the CNS[7], and its expression is regulated by Zfp24[19] and Chd7[20]. Sp7 is a C2H2 zinc finger transcription factor known to be crucial for osteoblast differentiation and bone formation[21]. *Sp7*-null mice die at birth due to an absence of bone formation[22].

Therefore, the role of Sp7 in oligodendrocyte maturation and CNS myelination, which occur postnatally in mice, remains unknown.

Here, we show that Sp7 has a cell-autonomous role in oligodendrocyte lineage cells where it mediates the expression of ECM related genes, and genes important for node of Ranvier formation. Oligodendrocyte-specific ablation of Sp7 resulted in aberrant node of Ranvier formation and in brain stiffness changes. Mechanistically, Sp7 acts on enhancers in open chromatin, where it modulates Sox10 binding and activates the expression of target genes. Our comparative analysis of DNA-binding and RNA expression in bone forming cells and in oligodendrocyte lineage cells suggests that Sp7 plays a conserved biological role in both cell lineages, where it mediates tissue stiffness by controlling the expression of ECM related genes.

Together, our results reveal mechanistic insights into how oligodendrocytes contribute to brain ECM and how this affects brain stiffness. Changes in ECM composition impedes remyelination[23], and aging related changes in brain stiffness inhibit oligodendrocyte lineage cell differentiation and impede remyelination[24]. Here we show that oligodendrocyte lineage Sp7 mutants fail to remyelinate normally when Sp7 is inactivated in adult oligodendrocyte progenitor cells (OPCs). Our study describes a novel pathway that could potentially be targeted to enhance remyelination in aging and in disease.

Results:

Sp7 is required for developmental myelination

The transcription factor Sp7 is expressed in the CNS solely by oligodendrocyte lineage cells[7]. To explore its role in these cells, we used the Cre-lox system to inactivate the mouse *Sp7* gene specifically in oligodendrocyte lineage cells. For oligodendrocyte-specific ablation of Sp7, we used mice with the Sp7 conditional allele[25] in combination with the Olig2-Cre line[26], resulting in $Sp7^{fl/fl}$;Olig2-Cre mice. We verified ablation of Sp7 in oligodendrocyte lineage cells using RNA-scope (Fig. S1). To explore the effect of oligodendrocyte-specific Sp7 ablation, we examined myelin and oligodendrocyte lineage cells in the $Sp7^{fl/fl}$;Olig2-Cre mice. We found that Sp7 ablation resulted in aberrant developmental myelination in the optic nerve of 15-day old mutant mice. Non-compact myelin loops were present in the mutant beneath and inside compact internodal myelin, and in residual myelin sheaths that incompletely covered the axon (Fig. 1A-D). This was accompanied by axonal swelling (Fig. 1E), that was observed only in $Sp7^{fl/fl}$;Olig2-Cre mice. At peak developmental myelination in mice (P21), normal appearing myelin was observed in the mutant (Fig. 1F-I). Nevertheless, Sp7 ablation caused hypomyelination, characterized by mild reduction in percentage of myelinated fibers (Fig. 1F-H), accompanied by slight reduction in density of mature oligodendrocytes (Fig. 1I-K). To explore the consequences of having reduced numbers of mature oligodendrocytes, we further explored the population of OPCs in the mutant and found an increased proliferation (Fig. 1L-N).

To explore if the reduced number of oligodendrocytes and hypomyelination we observed in $Sp7^{fl/fl}$;Olig2-Cre mice resulted in motor deficits, we performed gait analysis on three-month old mice. At this age, there was no difference in density of mature oligodendrocytes

in the mutant, and there was no evidence of microgliosis (Fig. S2). Gait analysis was performed using the DigiGait system in which a high-speed digital camera captures paw movement as mice walk on a treadmill at walking speeds of 10, 17 and 24 cm/second. While mutants did not have a profound motor phenotype, abnormal gait was detected in $Sp7^{fl/fl}$;Olig2-Cre mice, indicating that oligodendrocyte-specific ablation of *Sp7* results in motor abnormalities that persist into adulthood (Fig. 1O-P).

Sp7 is required for myelin maintenance and for remyelination

Based on Sp7's role in developmental myelination, we hypothesized that it might also be involved in myelin maintenance and remyelination. To differentiate between the developmental role of Sp7 with its potential role in adults, we used an inducible Cre-lox system, where developmental myelination remained intact. To explore the role of Sp7 in myelin maintenance, we used mice with the Sp7 conditional allele in combination with the inducible PLP-CreER^t line[27] that mediates recombination in mature oligodendrocytes, resulting in $Sp7^{fl/fl}$;PLP-CreER^t mice. Using this line, we found that at three months post-Sp7 ablation in adult animals, aberrant myelin was present in optic nerve of mutant mice, in which loops of non-compact myelin were present beneath compact internodal myelin (Fig. 2A-C). This was accompanied by the presence of phagocytic cells with myelin debris (Fig. 2D), and microgliosis (Fig. S2).

We next tested the effect of oligodendrocyte-specific ablation of Sp7 on remyelination. For the remyelination studies we used the cuprizone model of CNS demyelination. In this protocol, demyelination is induced by feeding mice with chow containing 0.2% cuprizone for 6 weeks. Remyelination is generally analyzed 2-3 weeks following removal of cuprizone from the animals' chow. For these studies we used the Sp7 conditional allele in combination with the inducible PDGFRα/CreER^T line[28] that mediates recombination in OPCs, resulting in *PDGFRα/CreER^T:Sp7$^{flox/flox}$* mice. To induce demyelination, 8-week-old *PDGFRα/CreER^T*–positive mice and *Sp7$^{flox/flox}$* mice (used as controls) were placed on 0.2% cuprizone chow for six weeks. To induce *Sp7* inactivation by the inducible *PDGFRα/CreER^T*, Cre positive and Cre negative animals were injected with tamoxifen for five days, two weeks prior to cuprizone exposure. After six weeks on cuprizone, all animals were placed on normal chow for three weeks to allow for remyelination. Following the remyelination period, the corpus callosum was assessed by EM. We found that while myelin thickness (g-ratio) was similar between WT and mutant upon remyelination (Fig. 2E-G), Sp7-specific ablation substantially reduced the percentage of myelinated fibers and caused aberrant remyelination in which non-compact myelin loops were present beneath compact internodal myelin (Fig. 2H).

Sp7 controls the expression of genes involved in node of Ranvier and ECM formation

Sp7 controls expression of transcripts important for ECM in bone forming cells[21,29-34]. Based on this, we hypothesized that Sp7 ablation would change expression of ECM transcripts in oligodendrocytes as well. To identify Sp7-regulated genes in oligodendrocytes, we cultured primary oligodendrocyte lineage cells derived from $Sp7^{fl/fl}$;Olig2-Cre mice and from Cre negative animals, used as controls, and collected total RNA and protein samples. Primary cultured oligodendrocytes derived from $Sp7^{fl/fl}$;Olig2-Cre mice had reduced MBP

and MAG protein levels, while having relatively normal levels of MYRF and OLIG2, confirming that these Sp7-ablated cells were still committed to the oligodendrocyte lineage (Fig 3A-C). RNA-seq of primary cultured mature oligodendrocytes revealed that Sp7 ablation changed expression of major transcripts that are crucial for ECM, oligodendrocyte interactions with the ECM, and for cholesterol synthesis (Fig 3D). Among differentially expressed genes (DEGs) were several collagens, integrins, proteoglycans and laminins (Supplemental RNA-seq data, Table S1). Among categories that were enriched in DEGs were “ECM organization”, “laminin interactions”, “ECM proteoglycans” and “non integrin membrane ECM interactions” genes (Fig. 3E). To further explore the importance of DEGs to ECM, we analyzed DEGs against the matrisome database[35]. This analysis revealed that oligodendrocyte-specific ablation of Sp7 changes the expression of 53 core matrisome transcripts and 128 matrisome-associated transcripts (Fig. 3F and Table S2). Among oligodendroglial DEGs detected upon Sp7 ablation were transcripts that encode components of the node of Ranvier, such as *Cntn2* (Tag-1), *Mal, Opalin, Cldn11,* and *Dcc*[36-40], and several transcripts that constitute perinodal ECM such as Versican (*Vcan*) and Hapln2 (*Bral1*)[11,41-44]. Sp7 ablated oligodendrocytes displayed reduced expression of the transcript that encodes the perinodal ECM protein tenascin R (*Tnr*), which is expressed in brain solely by oligodendrocyte lineage cells[7]. To validate the RNA-seq results in vivo, we examined TNR expression in brains of 21-day-old mutant mice. In line with the RNA-seq data, we found marked reductions in TNR protein expression in brains of $Sp7^{fl/fl}$;Olig2-Cre mice (Fig. 3G-H).

In vitro, oligodendrocyte conditioned media (OCM) induces formation of early nodal protein clusters (known as prenodes) along axons of retinal ganglion cells[45,46] and hippocampal neurons[9], independent of myelination. The ability of OCM to induce sodium channel clustering in neuronal cells is mediated by proteins, including TNR, secreted by oligodendrocytes into the media[8]. To functionally explore the role of Sp7 in prenode formation, we examined the sodium channel clustering activity of OCM derived from *Sp7*-ablated cells. We found that OCM derived from *Sp7*-ablated oligodendrocytes had reduced sodium channel clustering activity in cultured hippocampal neurons compared to OCM from control oligodendrocytes (Fig. 3I-N).

Sp7 is crucial for node of Ranvier integrity, and for brain stiffness

Brain ECM is concentrated in perineuronal nets (PNNs), axonal initial segments, and around nodes of Ranvier. This ECM plays an important role in determining mechanical and physiological properties of the brain[16]. TNR is an important component of brain ECM[47] and it concentrates in PNNs and around the node of Ranvier[42] (Fig. S3). Based on reduced expression of *Tnr* in Sp7-ablated oligodendrocytes (Fig. 3D) and in brains of Sp7 ablated animals (Fig. 3G-H), we hypothesized that PNN and node of Ranvier, in which TNR plays a structural role, may be affected. To test our hypothesis, we explored TNR expression in lumbar spinal cord of $Sp7^{fl/fl}$;Olig2-Cre mice. In spinal cord grey matter, we found reduced expression of TNR in the PNN. Reduced expression of TNR however, did not affect the distribution of PNN in brains of $Sp7^{fl/fl}$;Olig2-Cre mice (Fig. S3). In spinal cord white matter, we found reduced TNR expression at nodes of Ranvier (Fig. 4A-C).

Brain stiffness depends mainly on ECM, and not on myelin[48,49]. To explore whether aberrant expression of ECM related transcripts changed the brain's mechanical properties, we used atomic force microscopy (AFM) to measure brain stiffness. We found that oligodendrocyte-specific ablation of Sp7 resulted in reduced brain stiffness in the corpus callosum and cortex (Fig. 4D). To explore the effect of Sp7 ablation on node of Ranvier formation, we examined nodal, paranodal and juxtaparanodal areas in mutants by electron microscopy (EM) and by immunohistochemistry (IHC). EM revealed that Sp7 ablation results in abnormalities in paranodal organization (Fig. 4E-I). Splitting of compact myelin in paranodal areas was observed in the mutant (Fig. 4F), as well as abnormal formation of paranodal loops oriented away from the axolemma (Fig. 4H). In addition, increased nodal length and reduced nodal destiny were observed in brains, optic nerves and spinal cords of mutant mice, as observed by IHC (Fig. 4 J-O) and EM (Fig. 4 P-Q). Taken together, these data indicate that Sp7 plays a critical role in formation of node of Ranvier ECM and in determination of brain stiffness. To examine the mechanism by which Sp7 mediates these biological activities, we sought next to explore binding of Sp7 to the genome.

Sp7 enhancers in oligodendrocyte lineage cells

To focus on direct Sp7-target genes in oligodendrocyte lineage cells, we performed chromatin immunoprecipitation sequencing (ChIP-seq) analysis by immunoprecipitating endogenously expressed Sp7 and associated chromatin from primary cultured mature oligodendrocytes, using an anti-Sp7 antibody. To corroborate this data, we also enforced expression of Flag-tagged Sp7 in mouse primary cultured oligodendrocyte and performed ChIP-seq analysis using an anti-Flag antibody (Fig. 5 and Fig S4). Consistent with other Sp7 ChIP-seq datasets derived from bone forming cells[21,31], we identified two main groups of Sp7 bound peaks, proximal and distal to the transcription start site (TSS) that represent promoters and distal enhancers (Fig. 5A-D).

Sp7 distal enhancer peaks were enriched in genes associated with myelin formation and oligodendrocyte differentiation (Fig. 5E), and Sp7 promoters were enriched in genes associated with non-coding RNA metabolic processes (Fig. S4). In bone forming cells, Sp7 binds chromatin indirectly by associating with either Dlx family transcription factors (in osteoblasts)[21,31] or AP1 family members (in osteocytes)[31]. Based on this, we hypothesized that Sp7 has an oligodendrocyte-specific cofactor. De-novo motif analysis of Sp7 bound distal enhancers in oligodendrocytes identified the binding site of Sox family members as the most enriched motif (Fig. 5F, and Fig. S4). We intersected our RNA-seq and ChIP-seq datasets to identify 509 Sp7 target genes in oligodendrocytes (Fig. 5G). The most enriched categories in Sp7 target genes in oligodendrocytes are directly linked to the ECM. This was based on identifying 28 core matrisome genes and 97 matrisome-associated genes among the Sp7-target genes in oligodendrocytes (Fig. 5H). Our RNA-seq study revealed that transcripts that were differentially expressed upon Sp7 ablation were enriched for both ECM related genes and for genes important for cholesterol biosynthesis, which are regulated by sterol regulatory element binding proteins (SREBPs) (Fig. 3E). In contrast, Sp7 target genes were enriched mainly for ECM related genes (Fig. 5G), suggesting that reduced expression of genes related to cholesterol biosynthesis is a secondary effect caused

by altered ECM. Our data therefore suggest that in brain, the ECM is a direct effector of cholesterol biosynthesis related genes regulated by SRBPs, as observed by others[50,51].

Convergent and divergent Sp7 biological activities in the CNS and in bones

To systematically explore the effect of Sp7 ablation on the open chromatin landscape in mature oligodendrocytes, we performed ATAC-seq on primary cultured mature oligodendrocytes derived from $Sp7^{fl/fl}$;Olig2-Cre mice and Cre negative $Sp7^{fl/fl}$ mice (Fig. 6A). We found that Sp7 bound peaks fall within open chromatin sites in oligodendrocytes, but as expected, only a subset of open chromatin sites was Sp7 bound (Fig. S5). Our ATAC-seq revealed that ablation of Sp7 does not cause a significant change in the open chromatin landscape in mature oligodendrocytes (Fig. 6A), but rather acts upon open regulatory regions, in a similar fashion to the way Sp7 acts during the transition from osteoblasts to osteocytes[31].

We therefore sought next to explore the effect of Sp7 on genome-wide binding dynamics of other transcription factors within open chromatin[52]. To do so, we focused on Sp7 distal enhancers that are in open chromatin (coincide with ATAC-seq peaks) and compared transcription factor-footprinting before and after Sp7 ablation on these distal peaks that bind Sp7 in WT oligodendrocytes (Fig. 6B). This footprint analysis revealed that the binding motif of Sox transcription factors was less protected in Sp7 ablated cells, suggesting that ablation of Sp7 reduced binding of Sox transcription factors in Sp7 bound open regions. This was observed for Sp7 distal enhancers, but not in Sp7 proximal enhancers (Fig. S6).

Our de-novo motif analysis of Sp7 bound enhancers in oligodendrocytes identified the binding site of Sox9 and Sox10 as the most enriched motif in Sp7 peaks (Fig. 5F), which was based on the similarity in their binding motif (Fig. S4). Nevertheless, since Sox9 is not expressed in oligodendrocytes[7], we focused here on Sox10, which is known to play an essential role in mature oligodendrocytes. The Sox10 motif was in the center of Sp7 bound sites (Fig. 6C), suggesting that Sox10 may represents an oligodendrocyte-specific cofactor of Sp7 (See example of Sox10 peak in Sp7 peak in Supplemental Figure S6). Using the ATAC-seq footprinting analysis we explored how Sp7 ablation affects the binding of transcription factors Sox10 and CCCTC-Binding Factor (CTCF, as control) in Sp7 distal enhancers (Fig. 6D-E). Our analyses revealed that ablation of Sp7 substantially reduced the Sox10 footprint in distal enhancers of Sp7, but barely affected binding of CTCF in the same set of ATAC peaks, suggesting that Sp7 ablation has a specific effect on Sox10 binding (Fig. 6D-E). To further test this possibility, we divided Sox10 bound peaks into two groups: peaks in which binding of Sox10 coincides with Sp7, and Sox10 peaks in which we did not detect Sp7 binding (Fig. 6F). We explored how Sp7 ablation affects Sox10 binding in these two groups of Sox10 peaks. We found that ablation of Sp7 changes the aggregated signal of Sox10 binding only in Sox10 peaks that were Sp7 positive (Fig. 6G) but had no effect on Sox10 peaks that were Sp7 negative (Fig. 6H). Expression of Sox10 does not change upon Sp7 ablation (Fig. 3, and supplemental RNA-seq data). Therefore, this analysis strongly suggest that Sp7 ablation weakens the association of Sox10 with DNA in a defined set of enhancers (Sox10 & Sp7 positive) in mature oligodendrocytes, either directly or indirectly.

To further understand the role of Sox10 and Sp7 positive enhancers in oligodendrocytes, we examined genes associated with them. This set of genes was enriched for genes important for cell adhesion and node of Ranvier, such as *Cntn2*, (Fig. 6I), suggesting that binding of Sp7 to these specific sites can explain the abnormalities of the node of Ranvier observed in the mutant (Fig. 4). To understand how Sp7 ablation affects expression of these genes, we focused on the 230 genes that had Sox10 and Sp7 binding and were also differentially expressed upon Sp7 ablation. We found that these genes were enriched for cell adhesion genes that are important for the organization and interaction with the ECM, such as *Tnr* and laminin *Lama1* (Fig. 6J).

Our data suggest that in oligodendrocytes Sp7 directly regulates expression of genes related to the ECM (Fig. 5G). To explore if Sp7 has a similar biological role in bone forming cells, we explored Sp7-target genes that are differentially expressed upon Sp7 ablation or overexpression (by RNA-seq) and have Sp7 binding (by Sp7 ChiP-seq) in osteocytes and in osteoblasts[31]. We found that in both osteocytes (Fig. 7A) and osteoblasts (Fig. 7B) Sp7 target genes are enriched primarily for ECM related genes. Since we found that Sp7 target genes in oligodendrocyte are also enriched primarily for ECM related genes, this data suggest Sp7 has a similar biological function in oligodendrocytes and in bone forming cells. Nevertheless, the ECM in brain and bones is different in its components and in its biomechanical properties. To further understand the cause for the similarities in Sp7 function in these cells, we compared all Sp7-bound sites in oligodendrocytes with published Sp7 Chip-seq data in primary osteoblasts (POBs)[21,31] and osteocytes (Ocy)[31]. We found that 235 of the Sp7-bound distal enhancers in oligodendrocytes were also Sp7 bound in bone forming cells, mainly in osteocytes (Fig. 7C). To further understand the importance of Sp7 bound sites that were bound in both oligodendrocyte and in osteocytes, we compared direct Sp7-target genes in these two lineages. This comparison revealed that in both cell lineages, Sp7 directly controls the expression of transcripts that are crucial for the ECM (Fig. 7D).

Taken together, these observations suggest that Sp7 regulates the expression of ECM related genes in osteocytes and osteoblasts (in bones), and in oligodendrocytes (in the brain). To mediate ECM related gene expression in a cell lineage specific context, Sp7 was found to interact with DLX in osteoblasts and with AP1 in osteocytes (Fig. 7E-F), to act together in open chromatin[21,31,53]. Our data suggest that in mature oligodendrocytes, Sp7 acts in open chromatin, where it changes Sox10 binding to a group of enhancers that regulate genes important for the formation of the brain-specific ECM and node of Ranvier, thereby controlling node of Ranvier formation and brain stiffness (Fig. 7 G-H).

Discussion

Brain ECM plays essential roles in CNS development and disease. In particular, oligodendrocyte lineage cell derived ECM components precisely regulate the formation of node of Ranvier and PNN. Here, we show that the transcription factor Sp7 is required in oligodendrocytes for developmental myelination, myelin maintenance, and for remyelination. By combining ChIP-seq data of Sp7 in oligodendrocytes with RNA-seq data of Sp7 ablated oligodendrocytes, we identified Sp7 target genes in mature oligodendrocytes. These genes include genes required for formation of node of Ranvier and brain ECM.

Accordingly, oligodendrocyte-specific ablation of Sp7 results in aberrant node of Ranvier formation and a general reduction in brain stiffness, as measured by AFM. Based on this, we conclude that Sp7 is a transcription factor that promotes node of Ranvier and brain ECM formation by regulating expression of ECM and node of Ranvier related genes in oligodendrocyte lineage cells.

We have previously shown that oligodendrocytes maintain sodium channel clusters in nodes of Ranvier, independent of myelin[54]. This is supported by recent studies suggesting that oligodendrocytes induce the clustering of voltage-gated sodium channels in a step that precedes developmental myelination[9] by secreting TNR and other ECM proteins[8]. Together, these studies suggest that oligodendrocyte-secreted ECM proteins control node of Ranvier formation independent of myelin formation. Nevertheless, while the transcriptional control of myelin genes in oligodendrocyte lineage cells has been studied extensively[12,14] the transcriptional control of ECM and nodal genes in oligodendrocytes has remained elusive.

Node of Ranvier assembly in the CNS involves three mechanisms: (1) secreted glia-derived ECM complex proteins that cluster sodium channels, (2) formation of paranodal axoglial junctions that act as barriers to maintain nodal proteins in place, and (3) changes in axonal cytoskeletal scaffolds that maintain sodium channels at nodes[11]. Our data suggest that Sp7 is involved in the first two mechanisms by controlling expression of oligodendrocyte-secreted ECM proteins that are directly involved in nodal formation such as *Tnr*[47], *Hapln2* (Bral1)[43], *Versican*[42], and *Olfactomedin 2*[8], and by controlling expression of paranodal loop structural components such as *Cntn2* (Tag-1)[39], and *Opalin*[40]. Paranodal region adhesion molecules control myelin growth and internode length[55], therefore it is possible that by controlling nodal ECM and paranode formation, Sp7 also controls internodal myelin stability. This possibility is supported by our observation that Sp7 participates in myelin maintenance (Fig. 2).

We also explored the mechanism by which Sp7 controls expression of ECM and nodal genes in oligodendrocytes. Our ATAC-seq data revealed that Sp7 does not globally change the open chromatin landscape upon oligodendrocyte differentiation, but rather acts upon open regulatory regions, where it mediates Sox10 binding to specific active enhancers of ECM and nodal genes. Sox10 is a transcription factor that facilitates expression of myelin genes in Schwann cells in the PNS[56,57] and in oligodendrocytes in the CNS[58]. In addition to mediating both CNS and PNS myelination, Sox10 controls expression of genes important for node of Ranvier formation in the PNS. To do so, Sox10 interacts with the Schwann-cell-specific transcription factor Egr2 (Krox20)[59] and together these two transcription factors induce the expression of genes important for node of Ranvier formation[60]. The concurrent activation of both myelin genes and node of Ranvier genes by Sox10 ensures timely myelination and node of Ranvier formation in the PNS, while co-activation with Egr2 likely enables fine-tuning mechanisms for preference of myelin genes versus nodal genes[60]. Here we found that in oligodendrocytes, Sp7 binds in proximity to genes important for ECM and node of Ranvier formation (Fig. 5), where it changes chromatin accessibility in a subset of Sox10 binding sites (Fig. 6).

In brain, Bral1 (Hapln2) dependent ECM concentrates around node of Ranvier, and Bral2 (Hapln4) dependent ECM concentrates in PNN[43,61]. Both Bral1 and Bral2 where differentially expressed in Sp7 ablated oligodendrocytes, suggesting that the ECM in PNN is also directly controlled by Sp7. The Sp7 targets *Tnr, Tnc,* and versican (*Vcan*) play fundamental roles in constructing the PNN[47,62]. In addition, Sp7 targets in oligodendrocytes include enzymes that are important for PNN formation, including disintegrin and metalloproteinase with thrombospondin motifs 4 (*Adamts4*), and sulfotransferases *Chst1* and *Chst11*[4,63,64]. In line with the transcriptomic data, our data suggest that oligodendrocyte-specific Sp7 ablation affects PNN formation in spinal cord (Fig 4). Sp7 is the only transcription factor that is directly linked to PNN formation.

Sp7 belongs to the Sp family of transcription factors[22], which are known to bind to GC-rich motifs[21,53,65-68]. During evolution from protochordates to jawed fish, the Sp7 gene acquired changes that allowed its interaction with other factors, resulting in its binding to AT-reach motifs[21]. These changes enabled binding of Sp7 to DLX and to AT-rich motifs. This change in Sp7 binding motif is an important factor in transcriptional programing that enabled bone formation during evolution. In parallel, changes in the genes Olig1, Olig2 and Myrf, accumulated during evolution. This established the transcriptional program that enabled the formation of myelin, which also appeared first in jawed fish[69,70]. Our findings that the most enriched motif in the Sp7-bound peaks in oligodendrocytes is a Sox motif (AT-rich) suggest that the evolutionary change in Sp7 binding from GC-rich to AT-rich motifs played an important role not only in bone formation, but also in the formation of brain ECM. Interestingly, the disease-related human mutation S309W in the Sp7 gene changes the binding specificity of Sp7 from AT-rich motifs back to GC-rich motifs and results in aberrant ECM gene expression. This mutation, which in a way reverses the evolution of the Sp7 gene, results in human patients with craniosynostosis, cranial hyperostosis, and long bone fragility[53]. It would be very interesting to explore how this mutation affects oligodendrocyte gene expression, nodes of Ranvier development, PNN formation, and saltatory conduction.

In osteoblasts, Sp7 mediates gene expression by interacting with its cofactor DLX. In osteocytes, Sp7 mediates gene expression by interacting with its cofactor AP1 (FOS;JUN). Our data suggest that in oligodendrocytes, Sp7 mediates gene expression by interacting with Sox10 (Fig. 6). Based on this, we propose a model in which Sp7 interacts with a cell specific cofactor, thus mediating ECM related gene expression in a cell-type specific manner (Fig. 7). The evolutionary changes in Sp7 that allowed its interaction with other transcription factors, changed its DNA binding motif[21]. Changes in gene regulatory networks are a driving force of developmental and evolutionary processes[71,72]. Our study demonstrates how integration of Sp7 into different gene regulatory networks may have contributed to parallel bone and brain developmental and evolutionary changes.

Brain stiffness plays a fundamental role in nearly all biological processes in the CNS, including development, regeneration, and aging. Establishing accurate CNS biomechanics is an important but largely overlooked function of oligodendrocytes. In our study we used a combination of AFM, genetic, and transcriptional studies, to provide a detailed mechanism by which Sp7 controls the critical contribution of oligodendrocytes to CNS tissue stiffness.

Our data suggest that a similar biological activity of Sp7 that evolved separately in oligodendrocytes and osteoblast lineage cells plays a fundamental role in ECM formation of bone, cartilages, and CNS. The brain is the softest tissues of the body, whose mechanical properties rely on the molecular composition of its ECM, especially on low expression of Collagen-1 (*Col1a1* and *Col1a2*)[73]. Conversely, bones, which are the hardest body tissue, rely on high Collagen-1 levels to establish their characteristic stiffness[73]. Sp7 dictates bone stiffness by directly activating the expression of *Col1a1*[30] and *Col1a2*[33] in osteoblasts. In addition, Sp7 directly controls the expression of the less abundant type 5 collagen genes *Col5a1* and *Col5a1* that interact with type I collagen[32,34]. We report here that ablation of Sp7 in oligodendrocytes resulted in dramatic changes in ECM related transcripts (Fig. 3), including ECM components and ECM modifying enzymes (Fig. 3), resulting in changes in brain stiffness (Fig. 4). Taken together, these data suggest that Sp7 plays a fundamental role in controlling tissue stiffness in bones and the CNS by mediating expression of ECM genes.

The contribution of oligodendrocyte lineage cells to node of Ranvier formation is an intricate process that occurs before, during, and after myelination. Before node formation, ECM proteins secreted from oligodendrocytes mediate clustering of voltage-gated sodium channels[8] that later become nodes[10,74]. During myelination, formation of paranodal junctions maintain nodal proteins in place[11] and regulate internodal myelin growth[55]. Only after completion of developmental myelination does mature ECM appear around nodes[11]. Our data indicate that Sp7 controls these processes, and that the interaction of Sp7 with Sox10 on a specific set of enhancers enables fine-tuning for myelin versus ECM related gene expression.

Limitation of the study

The ECM in demyelinated lesions affects the ability of oligodendrocytes to remyelinate[75]. Recent studies demonstrate that oligodendrocytes not only respond to the ECM in demyelinated lesions, but also actively modify it[76]. Our data suggest that Sp7 is important in adults for both myelin maintenance and for remyelination, such that it is difficult to determine if the reason for remyelination failure is the aberrant ECM that was generated following Sp7 ablation, or a failure of the Sp7-ablated oligodendrocytes to respond to the ECM in the demyelinated environment.

Osteoblasts utilize the mechanosensitive channels Piezo1 and Piezo2 to activate the YAP/TAZ pathway which induces osteoblast differentiation and bone formation in response to mechanical forces[77]. Oligodendrocytes are also responsive to mechanical forces and use Piezo1 for mechanotransduction[24]. In addition to ECM related genes mentioned above, *Piezo1* and *Piezo2*, as well as the YAP/TAZ pathway transcription factor TEA domain family member 2 (*Tead2*) are differentially expressed in the Sp7 ablated oligodendrocytes, suggesting that remyelination failure in Sp7 ablated oligodendrocytes may result from the inability to respond to the stiffness of their environment. Further studies, using artificial matrixes with differential stiffness will be required to explore the effect of Sp7 ablation on mechanotransduction in oligodendrocytes.

In addition, further studies are required to explore why MBP and MAG translation fail in the primary cultured oligodendrocytes derived from Sp7-ablated cells. Transcript levels of these

genes were normal (Fig. 3), and the MBP staining in brain of Sp7 ablated animals appeared relatively normal (Fig. 1). Only at the protein level was there a reduction in MBP and MAG levels in vitro (Fig. 3). Similar phenomenon was observed in KLF9 mutants, in which oligodendrocytes that lacked the transcription factor KLF9 fail to express MBP in vitro, but were normal in vivo[78]. Among the differentially expressed genes in the Sp7 ablated genes were several integrins and laminins, which are known to control *Mbp* translation[79]. Further in vitro studies are needed to determine how Sp7, perhaps by controlling integrin expression, influences *Mbp* translation in vitro, and what mechanism(s) compensate for this and allow *Mbp* translation in vivo.

STAR Methods

RESOURCE AVAILABILITY

Lead Contact—Further information and requests for resources and reagents should be directed to and will be fulfilled by the lead contact, Brian Popko (brian.popko@northwestern.edu).

Materials Availability—The PLP-CreERt mice used in this study are available from Brian Popko (brian.popko@northwestern.edu) upon request.

Data and code availability

- The ChiP-Seq, ATAC-seq and RNA seq datasets have been deposited in the Gene Expression Omnibus (GEO) repository.

These datasets are publicly available, with accession number GEO: GSE221193 (https://www.ncbi.nlm.nih.gov/geo/query/acc.cgi?acc=GSE221193). This paper also analyzes previously published data[20] and[31]. This existing data are publicly available, and the accession numbers are listed in the Key Resources table.

- This paper does not report original code.
- Any additional information required to reanalyze the data reported in this paper is available from the lead contact upon request.

EXPERIMENTAL MODEL AND STUDY PARTICIPANT DETAILS

Mice—Animals used in this study were housed in pathogen-free conditions at controlled temperatures and relative humidity with a 12/12 hr light/dark cycle and free access to pelleted food and water. All animal experiments were conducted in accordance with the ARRIVE guidelines and in complete compliance with the guidelines of Northwestern University Institutional Animal Care and Use Committee (IACUC).

Mice for experiments were generated by crossing the $Sp7^{fl/fl}$ mice[25] (RRID:IMSR_JAX:035391) with either the Olig2-Cre mice[26] (RRID:IMSR_JAX:025567), or with the PLP-CreERt mice[27] (RRID:IMSR_JAX:005975), or with the PDGFRa-CreERt2 mice[28] (MGI:3832569), resulting in $Sp7^{fl/fl}$;Olig2-Cre mice, $Sp7^{fl/fl}$;PLP-CreERt mice, and $Sp7^{fl/fl}$; PDGFRa-CreERt2 mice, respectively. In all the experiments, Cre negative $Sp7^{fl/fl}$ mice were used as controls.

All mouse lines were on the C57BL/6 background. The sex of the animal did not impact the levels of developmental myelination, and both female and male mice were used in all the studies. The mice used for all the studies were healthy (beside mild motor deficit in the $Sp7^{fl/fl}$;Olig2-Cre mice, described in Fig. 1) and were not used in previous procedures. The $Sp7^{fl/fl}$;Olig2-Cre mice were tested naïve. The $Sp7^{fl/fl}$;PLP-CreERt mice and the $Sp7^{fl/fl}$;PDGFRa-$CreER^{t2}$ mice were tested following tamoxifen injections. Six to eight weeks old mice were used for tamoxifen injections.

METHOD DETAILS

Tamoxifen injections—Tamoxifen injections were performed as we previously described[80]. One mg/day 4-hydroxytamoxifen (H-6278, Sigma) was injected for five consecutive days for $Sp7^{fl/fl}$;PLP-CreERt and $Sp7^{fl/fl}$; PDGFRa-CreERt2 mice.

Behavioral analyses—Gait analysis was performed using the DigiGait (Mouse Specifics Inc., Boston, MA) imaging system. In this system, a high-speed digital camera captured the movement of the paws as the mouse walked on a treadmill belt, and simultaneously analyzed various gait parameters. Each animal was tested on the DigiGait treadmill ten times on the day of testing, with 2-minute breaks in between. Data collection started after the animal walked consistently for at least 3 complete strides. Gait analysis was performed at walking speed of 10, 17 and 22 cm/second. Walk velocity was controlled by the DigiGait system by controlling the speed of the treadmill. Footprints from fluent runs with a steady velocity were analyzed. The behavioral studies were done blindly, such that the researcher who performed the DigiGait analysis was not aware of the genotype of the mice.

Cuprizone administration—To induce demyelination, $Sp7^{fl/fl}$; PDGFRa-$CreER^{t2}$ mice and Cre negative $Sp7^{fl/fl}$ mice (male and female) were used. To induce Sp7 ablation, six-weeks-old mice were injected with tamoxifen, as described above. Two weeks post tamoxifen injection, the mice were fed a 0.2% cuprizone diet (Envigo, Madison, WI, USA) for six weeks, as described[81]. The mice were then placed back on normal chow for three weeks to allow remyelination to occur. The corpus callosum of each mouse was collected after three weeks of remyelination on normal chow.

Electron microscopy (EM) analysis—Morphometric analysis was performed essentially as described previously[82-84]. Mice were perfused with saline, followed by perfusion with a solution of 2.5% glutaraldehyde and 4% paraformaldehyde in a 0.1 M sodium cacodylate buffer. Optic nerves and corpus callosum were harvested and postfixed in the same fixative at 4°C for two weeks, and were embedded in epoxy resin. Semithin sections were stained with toluidine blue and observed on a slide scanner microscope (Olympus, SlideView, VS200). Ultrathin sections were double stained with uranyl acetate and lead citrate and observed on an FEI Tecnai Spirit G2 transmission electron microscope. G-ratios were calculated from the EM images, as described in[85].

Immunohistochemistry and cell counts—Immunohistochemistry was essentially performed as previously described[80,82,86]. Mice were deeply anaesthetized with 2.5% avertin (Cat# T48402, Sigma Aldrich) in dH2O. Upon the loss of nociceptive reflexes, mice

were transcardially perfused with 0.9% saline followed by ice-cold 4% paraformaldehyde (PFA). Brains, spinal cord and optic nerves were collected and postfixed overnight in 4% PFA at 4°C, followed by incubation in 30% sucrose until saturation. Tissues were then embedded in OCT, sectioned at 10μm, and stained with indicated antibodies.

Primary mouse cell cultures—Mouse oligodendrocyte lineage cells (OPCs) were isolated from $Sp7^{fl/fl}$;Olig2-Cre mice and from $Sp7^{fl/fl}$ mice (used as a control) by the immunopanning method[87], as we previously described[19,84,86]. For OPC isolations, 6-8-days-old pups were used, both males and females. For proliferation media, platelet-derived growth factor-AA (PDGF-AA; 10 ng/ml, PeproTech #100-13A), neurotrophin-3 (1 ng/ml, PeproTech #450-03), forskolin (Sigma Aldrich [0.01 mM]), and ciliary neurotrophic factor (CNTF; 10 ng/ml, PeproTech #450-13) were added. To stimulate differentiation, PDGF-AA was removed and triiodothyronine (40 ng/ml, Sigma # T6397) was added. Media was changed every other day and differentiated cells were collected after five days in differentiation media. For OCM collection, mature oligodendrocyte derived the $Sp7^{fl/fl}$;Olig2-Cre mice or $Sp7^{fl/fl}$ mice were grown in neurobasal media for 48h. The OCM was collected, centrifuged to remove cells debris, if any, and filtered through a 0.22 μm filter.

Primary hippocampal neurons were isolated from neonatal (P0-P1) mice by standard techniques as we described previously[88], with minor modifications. Neonatal hippocampi were dissected out and their meninges removed in dissection media (10 mM HEPES in Hank's Balanced Salt Solution [HBSS]). Brain tissue was then minced and trypsinized (0.25% trypsin and 1% DNAse in HBSS media) in 37°C water bath for 15 minutes. Trypsinized tissue was then washed twice in culture media (1% L-glutamine, 1% penicillin/streptomycin, 2% B27, and 10% fetal bovine serum in Dulbecco's Modified Eagle Medium [DMEM]), followed by mechanical trituration in culture media. Dissociated cells were then plated on poly-D-lysine-coated glass coverslips and left to incubate at 37°C and 5% CO_2. 24 hours after plating, cells were treated with mitotic inhibitor (5 μM fluorodeoxyuridine [FUDR] in culture media) to arrest division of glial cells. 12 hours after, the mitotic inhibitor was washed out and cells were fed with culture media. OCM was added to the cultured hippocampal neurons at 3 days in vitro (DIV). One-third of the medium was changed with neurobasal medium (NM) at 7 DIV, and then twice a week. The cells were fixed at 21 DIV.

The primary cultures were taken from healthy mice that were (1) not involved in previous procedures and (2) were not treated with drugs.

Immunocytochemistry and Sodium channel clustering analysis—Sodium channel clustering analysis was done as described in[8]. Cells cultured on coverslips were rinsed with PBS and fixed in ice cold 4% PFA for 10 min at RT, washed with PBS, then air-dried and stored at −80°C until immunostaining with the indicated antibodies.

Images were acquired using A1R laser scanning confocal microscope. Z-series sections were performed at 0.3 μm increments. Maximum orthogonal projections of images were used to plot profiles of immunofluorescence intensity, using Fiji software (NIH, Bethesda, Maryland). At least 35 neurons per coverslip, identified by NFM and AIS, were counted,

and the percentage of neurons with sodium channel clusters was determined for at least three coverslips per condition (total of at list 115 neurons per condition, from three cover slips). Sodium clusters were defined by a length of >1μm, and mean value of cluster area was at least 2.5 that of the adjacent region of the axon. Cluster length was measured on the plot profiles and was measured at half-height of the fluorescence peak.

RNA-scope—RNA scope was performed as previously described[84]. A mouse Myrf mRNA probe (ACDbio, Cat# 524061) was used with a mouse Sp7 mRNA probe (ACDbio, Cat# 403401) using the RNAscope Multiplex Fluorescent Reagent Kit V2 Assay (ACDbio, Cat# 323110) (ACDbio). Fluorophores were purchased from Akoya Biosciences (Opal 520: Cat# FP1487001KT, Opal 620: Cat# FP1495001KT). Mice were processed for RNAscope assays as follows: deeply anesthetized animals were transcardially perfused with 0.9% saline followed by ice-cold 4% PFA as described above. Brains were immediately dissected out and transferred to 10% NB formalin solution (Sigma, Cat# HT5011) at RT for exactly 24 h. Brains were then transferred to freshly made 70% ethanol for 24 h at RT and processed for paraffin embedding. Sections were cut at 5 μm. RNAscope assays were performed as per the kit manufacturer's specifications.

Total protein isolation—Cells in culture were rinsed twice with sterile PBS, then lysed with ice-cold RIPA buffer containing protease inhibitors (Thermo Fisher Scientific, Cat# 78430) and phosphatase inhibitors (Sigma, Cat# P2850 and P5726) (lysis buffer), scraped and then collected in microcentrifuge tubes for a 10 min incubation on ice. Cell lysates were then centrifuged at 13,000 g for 15 min at 4°C, and the supernatant was collected and stored at −80°C until measurement. To collect brain tissues, mice were deeply anesthetized with 2.5% avertin and perfused with ice-cold sterile PBS, followed by brain isolation into microcentrifuge tubes and immediately frozen in liquid nitrogen. Brain samples were then stored at −80°C until homogenization. Brain tissue protein lysates were homogenized in lysis buffer, incubated on ice for 15 min and centrifuged at 13,000 g for 15 min at 4°C, with supernatants then being collected. Protein concentration was determined by using a BCA protein assay kit (Thermo Fisher Scientific, Cat# 23255) as per the manufacturer's instructions.

Western blot—Protein lysates were boiled for 5 min in Laemmli sample buffer (Bio-Rad, Cat# 161-0737) with β-mercaptoethanol (Sigma, Cat# M6250), separated by SDS-PAGE, transferred onto a nitrocellulose membrane and immunoblotted. The primary antibodies used were anti-TNR (R and D Systems: cat #MAB1624); Rabbit-anti-MBP (1:1000, Abcam, Cat# ab40390), rabbit-anti-MAG (1:1000, Thermo Fisher Scientific, Cat# AB_2533179), mouse-anti-Olig2 (1:1000, Millipore, Cat# MABN50), mouse-anti-MYRF (1:5000, a kind gift from Dr. Ben Emery), and GAPDH (1:2000, Cell signaling, Cat# 2118S). Western blot bands were analyzed using Image Lab software (Bio-Rad laboratories).

RNA isolation and RNA-seq—Total RNA was isolated from primary cultured oligodendrocytes using RNA isolation kit, following manufacture's protocol (Bio-Rad, Cat# 732-6820). RNA quality was confirmed by 2100 Bioanalyzer using a model 6000 Nano kit (Agilent technologies, Cat# 5067-1511). Samples with RNA integrity number > 8 were

used. Bulk RNA-seq was performed as we previously described[19,80,86]. RNA libraries were prepared using Illumina Total RNA-Seq Library Prep kit (Illumina Cat# 20020596) and sequenced by Illumina HiSeq 4000 sequencers using HiSeq Kit (illumine, Cat# 20024906), at the Northwestern University Next Generation Sequencing Core facility.

Subsequent Analysis of the RNA-Seq Data—Sequence reads were trimmed for adaptor sequence/low-quality sequence using trimgalore/0.6.7 and cutadapt/3.4. (https://github.com/FelixKrueger/TrimGalore). Trimmed sequence reads were mapped to mm10 using STAR version 2.7.10a with default parameters[89]. PCR duplicates and low quality mapped reads were removed using Picard and SAMtools respectively[90]. Number of reads (counts) associated with each gene were performed using featureCounts[91] and the differentially expressed features from the count tables were determined using the Deseq2 R package[92].

ChIP-seq—ChIP-seq was performed as previously described[86] on primary cultured mature oligodendrocytes, following the Sp7 Chip-seq protocol established by[21]. To get mature oligodendrocytes, primary cultured oligodendrocytes were cultured for five days in differentiative conditions (−PDGF, +40 ng/mL triiodothyronine; Sigma-Aldrich). The cells were washed with PBS (to remove cell debris), fixed in 1% PFA for 10 min, incubated with glycine, and were then flash frozen. The ChIP was then performed on formaldehyde cross-linked chromatin (~50 μg/sample) using an anti-Sp7 antibody (Abcam, ab22552) or anti-Flag antibody (Sigma F1804), as described in[93]. ChIP samples were used for Illumina library construction, and libraries were submitted to 75-base Illumina sequencing (>20 million reads/sample). The 75 nt sequence reads were mapped to the mouse genome (mm10) assembly using the BWA algorithm (default settings)[94].

Subsequent analysis of the ChIP-Seq data—Peak calling was performed with HOMER[95] using only uniquely mapped reads with PCR duplicates removed. The peaks were calculated (HOMER findPeaks –style factor) against input DNA as a control.

For de novo motif discovery, sequences of identified Sp7 peaks from HOMER were submitted to the MEME-ChIP suite[96]. GREAT[97] was used to find enriched annotations with the gene association rule set to basal + up to 100 kb. Occurrence of overlapping peaks of Sp7 in osteocytes and osteoblasts[31] were identified using findOverlaps from the GenomicRanges R package[98].

Cutadapt and FastQCcommands were used for adapter and quality trimming of raw reads using Trim Galore v0.6.7. (https://github.com/FelixKrueger/TrimGalore). The trimmed reads were then aligned to the UCSC mm10 genome using Bowtie2 version 2.4.5[99]. Alignments with MAPQ smaller than 5 were filtered and only uniquely/primary mapping reads were retained using SAMtools v1.14[90]. PCR duplicates were removed using Picard v2.26.10. Peak detection was carried out with HOMER version 4.11[95] findPeaks command were used with factor style for the chip compared to the input file. findMotifs.pl command was used to identify enriched motifs within the called peak list. BigWig files were generated using deepTools package version 3.5.1[100]. with the help of the bamCoverage command and the resulting BigWig files were normalized using the RPKM option. Other options

applied were '--binSize 20', '--extendReads' and '--centerReads' for highest resolution. The computeMatrix command was used to calculates scores per genome regions together with mm10 blacklist to exclude problematic regions from the score matrix. Heat maps were generated with plotHeatmap command.

ATAC-seq—Primary cultured oligodendrocytes derived from brains of $Sp7^{fl/fl}$; Olig2-Cre mice and Cre negative $Sp7^{fl/fl}$ mice (used as controls) were cultured as described above. OPCs that were grown in differentiation media for three days were used for premature oligodendrocytes, and OPCs that were grown for five days in differentiation media were used for mature oligodendrocytes. ATAC-seq libraries preparation was performed using the ATAC-seq Kit (Active Motif cat#53150) according to manufacturer's instructions. The libraries were sequenced at the NGS Core Facility of Northwestern University, using Illumina NextSeq 500, 1x75 bp, with 50 million reads per sample.

Subsequent analysis of the ATAC-seq data—Reads with low-quality base calls are trimmed off from the 3′ end with a phred score > 20, using Trim Galore v0.6.7 (https://github.com/FelixKrueger/TrimGalore).The reads were aligned to the UCSC mm10 genome using Bowtie2 version 2.4.5[99]. Alignments with low quality score were filtered out and only uniquely mapping reads with at most two mismatches were retained using SAMtools v1.14[90]. Peak calling was carried out with MACS2 version 2.2.7.1[101]. Callpeak command were used with mm10 as the genome and both treatment and control specified. To identify differential regions, we used MACS2 sub commands: predictd, callpeak, and bdgdiff. This results in three sets of regions, either specific to one or the other sample, or common to both. BigWig files were generated using deepTools package version 3.5.1[100] with the help of the bamCoverage command and the resulting BigWig files were normalised using the RPKM option. The ATAC-seq replicate samples were combined in order to produce the processed data files.

ATAC-seq DNA footprint analysis—ATAC-seq footprinting analysis was performed using TOBIAS (Transcription factor Occupancy prediction By Investigation of ATAC-seq Signal), essentially as described in[52]. TF motifs were downloaded from JASPAR CORE 2018[102], the JASPAR PBM HOMEO collection and Hocomoco V11 databases[103]. JASPAR motifs were linked to Ensembl gene IDs by mapping the provided Uniprot ID to the Ensembl gene ID through biomaRt43. Hocomoco motifs were likewise linked to genes through the provided HGNC/MGI annotation. Footprint plots were generated by the TOBIAS visualization modules.

Atomic force microscope (AFM) measurements—Measurements of brain stiffness were performed as described in[49]. Animals were anaesthetized with 2.5% Avertin and the brains were removed and fixed in 4% paraformaldehyde for 16 hours. Coronal sections were sectioned to a thickness of 100 μm using a mouse brain mold, washed extensively with PBS, and stored at 4 °C in PBS. Force maps from the brain tissue were collected using a Bruker BioSoft Indenter system using 200-micron spherical probe at the Scanned Probe Imaging and Development facility (SPID) at the Atomic and Nanoscale Characterization Center (NUANCE) of Northwestern University. The force-indentation curves were fit to the

Hertz model[104] for spherical tips to determine Young's modulus, with an assumed Poisson's ratio value of 0.45 for the sample.

QUANTIFICATION AND STATISTICAL ANALYSIS

Statistical analyses including the number of animals, the number of replications, and P values for each experiment are noted in the figure legends. In all the experiments, Cre positive mice were used as study subjects, and littermate Cre negative $Sp7^{fl/fl}$ mice were used as controls. As the Cre positive and Cre negative mice are phenotypically indistinguishable, mice were stratified into groups based on age. For each age-group, the number of Cre positive and Cre negative mice and the age are noted in the figure legends. In all the experiments, all the animals in the study were used, and inclusion or exclusion criteria were not applied. For the immunohistochemistry and electron microscopy data, statistical significance was determined using two-tailed unpaired Student's t tests. A p value of less-than 0.05 was considered significant. Statistical tests were performed using Prism 8 software. No statistical methods were used to predetermine sample size or to determine whether the data met assumptions of the statistical approach. Each n value represents an individual animal or cell culture. Statistical significance for the RNA-seq data was analyzed by DESeq2 R package[92]. Fold change greater than 1.5 with FDR lower than 0.05 were considered significant. Statistical significance in the ChiP-seq and ATAC-seq studies was determined using MACS2 version 2.2.7.1[101] and HOMER version 4.11[95]. For peak calling using MACS2 version 2.2.7.1, peaks with p value lower than 1e-5 with enrichment greater than 3-fold (compared to background) were considered significant. For Homer peak calling, peaks with p-value lower than 1e-4 with enrichment greater than 4-fold (compared to background) were considered significant.

Supplementary Material

Refer to Web version on PubMed Central for supplementary material.

Acknowledgments

The authors would like to thank Dr. Gajendra Shekhawa from the Atomic and Nanoscale Characterization Center at Northwestern University for his skillful help with ATM analysis. The authors would like to thank Professor Hironori Hojo from the University of Tokyo, for kindly sharing his detailed Sp7-Chip-seq protocol, and the late Professor Benoit de Crombrugghe from MD Anderson Cancer Center for providing the Sp7 floxed mice. Behavioral assays were performed at the Northwestern University Behavioral Phenotyping Core Facility.

This research was supported by an R01NS067550 grant to B.E and B.P. In addition, B.P. is supported by NIH R01NS109372, R01NS099334, 1RF1AG072080 grants and by the National Multiple Sclerosis Society (RG-1807-32005) grant. B.P. is also supported by the Dr. Miriam and Sheldon G. Adelson Medical Research Foundation and the Rampy MS Research Foundation (BP). B.E. is also supported by the DOD W81XWH2210386 grant. M.P. is supported by NIH R35NS132349. A.D is recipient of the British council GROWTH fellowship and the Dr. Willem Been Legacy award. A.E. is supported by ICRF grant 01301. Imaging work was performed at the Northwestern University Center for Advanced Microscopy generously supported by NCI CCSG P30 CA060553 awarded to the Robert H Lurie Comprehensive Cancer Center.

References

1. Bunge MB, Bunge RP, and Pappas GD (1962). Electron microscopic demonstration of connections between glia and myelin sheaths in the developing mammalian central nervous system. J Cell Biol 12, 448–453. 10.1083/jcb.12.2.448. [PubMed: 13874658]

2. Courel MN, Marret S, Girard N, Chauzy C, Olivier A, Bertrand P, Delpech A, Laquerriere A, Asou H, and Delpech B (1998). Hyaluronectin is produced by oligodendrocytes and Schwann cells in vitro. J Neurocytol 27, 27–32. 10.1023/a:1006982802778. [PubMed: 9530997]

3. Garwood J, Garcion E, Dobbertin A, Heck N, Calco V, ffrench-Constant C, and Faissner A (2004). The extracellular matrix glycoprotein Tenascin-C is expressed by oligodendrocyte precursor cells and required for the regulation of maturation rate, survival and responsiveness to platelet-derived growth factor. Eur J Neurosci 20, 2524–2540. 10.1111/j.1460-9568.2004.03727.x. [PubMed: 15548197]

4. Kohnke S, Buller S, Nuzzaci D, Ridley K, Lam B, Pivonkova H, Bentsen MA, Alonge KM, Zhao C, Tadross J, et al. (2021). Nutritional regulation of oligodendrocyte differentiation regulates perineuronal net remodeling in the median eminence. Cell Rep 36, 109362. 10.1016/j.celrep.2021.109362. [PubMed: 34260928]

5. Song I, and Dityatev A (2018). Crosstalk between glia, extracellular matrix and neurons. Brain Res Bull 136, 101–108. 10.1016/j.brainresbull.2017.03.003. [PubMed: 28284900]

6. Yellajoshyula D, Pappas SS, Rogers AE, Choudhury B, Reed X, Ding J, Cookson MR, Shakkottai VG, Giger RJ, and Dauer WT (2021). THAP1 modulates oligodendrocyte maturation by regulating ECM degradation in lysosomes. Proc Natl Acad Sci U S A 118. 10.1073/pnas.2100862118.

7. Zhang Y, Chen K, Sloan SA, Bennett ML, Scholze AR, O'Keeffe S, Phatnani HP, Guarnieri P, Caneda C, Ruderisch N, et al. (2014). An RNA-sequencing transcriptome and splicing database of glia, neurons, and vascular cells of the cerebral cortex. J Neurosci 34, 11929–11947. 10.1523/jneurosci.1860-14.2014. [PubMed: 25186741]

8. Dubessy AL, Mazuir E, Rappeneau Q, Ou S, Abi Ghanem C, Piquand K, Aigrot MS, Thétiot M, Desmazières A, Chan E, et al. (2019). Role of a Contactin multi-molecular complex secreted by oligodendrocytes in nodal protein clustering in the CNS. Glia 67, 2248–2263. 10.1002/glia.23681. [PubMed: 31328333]

9. Freeman SA, Desmazières A, Simonnet J, Gatta M, Pfeiffer F, Aigrot MS, Rappeneau Q, Guerreiro S, Michel PP, Yanagawa Y, et al. (2015). Acceleration of conduction velocity linked to clustering of nodal components precedes myelination. Proc Natl Acad Sci U S A 112, E321–328. 10.1073/pnas.1419099112. [PubMed: 25561543]

10. Thetiot M, Freeman SA, Roux T, Dubessy AL, Aigrot MS, Rappeneau Q, Lejeune FX, Tailleur J, Sol-Foulon N, Lubetzki C, and Desmazieres A (2020). An alternative mechanism of early nodal clustering and myelination onset in GABAergic neurons of the central nervous system. Glia 68, 1891–1909. 10.1002/glia.23812. [PubMed: 32119167]

11. Susuki K, Chang KJ, Zollinger DR, Liu Y, Ogawa Y, Eshed-Eisenbach Y, Dours-Zimmermann MT, Oses-Prieto JA, Burlingame AL, Seidenbecher CI, et al. (2013). Three mechanisms assemble central nervous system nodes of Ranvier. Neuron 78, 469–482. 10.1016/j.neuron.2013.03.005. [PubMed: 23664614]

12. Elbaz B, and Popko B (2019). Molecular Control of Oligodendrocyte Development. Trends Neurosci 42, 263–277. 10.1016/j.tins.2019.01.002. [PubMed: 30770136]

13. Emery B, and Lu QR (2015). Transcriptional and Epigenetic Regulation of Oligodendrocyte Development and Myelination in the Central Nervous System. Cold Spring Harb Perspect Biol 7, a020461. 10.1101/cshperspect.a020461. [PubMed: 26134004]

14. Sock E, and Wegner M (2019). Transcriptional control of myelination and remyelination. Glia 67, 2153–2165. 10.1002/glia.23636. [PubMed: 31038810]

15. Huang CY, and Rasband MN (2018). Axon initial segments: structure, function, and disease. Ann N Y Acad Sci 1420, 46–61. 10.1111/nyas.13718. [PubMed: 29749636]

16. Krishnaswamy VR, Benbenishty A, Blinder P, and Sagi I (2019). Demystifying the extracellular matrix and its proteolytic remodeling in the brain: structural and functional insights. Cell Mol Life Sci 76, 3229–3248. 10.1007/s00018-019-03182-6. [PubMed: 31197404]

17. Pu A, Stephenson EL, and Yong VW (2018). The extracellular matrix: Focus on oligodendrocyte biology and targeting CSPGs for remyelination therapies. Glia 66, 1809–1825. 10.1002/glia.23333. [PubMed: 29603376]

18. Rasband MN, and Peles E (2015). The Nodes of Ranvier: Molecular Assembly and Maintenance. Cold Spring Harb Perspect Biol 8, a020495. 10.1101/cshperspect.a020495. [PubMed: 26354894]

19. Aaker JD, Elbaz B, Wu Y, Looney TJ, Zhang L, Lahn BT, and Popko B (2016). Transcriptional Fingerprint of Hypomyelination in Zfp191null and Shiverer (Mbpshi) Mice. ASN Neuro 8. 10.1177/1759091416670749.
20. He D, Marie C, Zhao C, Kim B, Wang J, Deng Y, Clavairoly A, Frah M, Wang H, He X, et al. (2016). Chd7 cooperates with Sox10 and regulates the onset of CNS myelination and remyelination. Nat Neurosci 19, 678–689. 10.1038/nn.4258. [PubMed: 26928066]
21. Hojo H, Ohba S, He X, Lai LP, and McMahon AP (2016). Sp7/Osterix Is Restricted to Bone-Forming Vertebrates where It Acts as a Dlx Co-factor in Osteoblast Specification. Dev Cell 37, 238–253. 10.1016/j.devcel.2016.04.002. [PubMed: 27134141]
22. Nakashima K, Zhou X, Kunkel G, Zhang Z, Deng JM, Behringer RR, and de Crombrugghe B (2002). The novel zinc finger-containing transcription factor osterix is required for osteoblast differentiation and bone formation. Cell 108, 17–29. 10.1016/s0092-8674(01)00622-5. [PubMed: 11792318]
23. Ghorbani S, and Yong VW (2021). The extracellular matrix as modifier of neuroinflammation and remyelination in multiple sclerosis. Brain 144, 1958–1973. 10.1093/brain/awab059. [PubMed: 33889940]
24. Segel M, Neumann B, Hill MFE, Weber IP, Viscomi C, Zhao C, Young A, Agley CC, Thompson AJ, Gonzalez GA, et al. (2019). Niche stiffness underlies the ageing of central nervous system progenitor cells. Nature 573, 130–134. 10.1038/s41586-019-1484-9. [PubMed: 31413369]
25. Akiyama H, Kim JE, Nakashima K, Balmes G, Iwai N, Deng JM, Zhang Z, Martin JF, Behringer RR, Nakamura T, and de Crombrugghe B (2005). Osteo-chondroprogenitor cells are derived from Sox9 expressing precursors. Proc Natl Acad Sci U S A 102, 14665–14670. 10.1073/pnas.0504750102. [PubMed: 16203988]
26. Kessaris N, Fogarty M, Iannarelli P, Grist M, Wegner M, and Richardson WD (2006). Competing waves of oligodendrocytes in the forebrain and postnatal elimination of an embryonic lineage. Nat Neurosci 9, 173–179. 10.1038/nn1620. [PubMed: 16388308]
27. Doerflinger NH, Macklin WB, and Popko B (2003). Inducible site-specific recombination in myelinating cells. Genesis 35, 63–72. 10.1002/gene.10154. [PubMed: 12481300]
28. Rivers LE, Young KM, Rizzi M, Jamen F, Psachoulia K, Wade A, Kessaris N, and Richardson WD (2008). PDGFRA/NG2 glia generate myelinating oligodendrocytes and piriform projection neurons in adult mice. Nat Neurosci 11, 1392–1401. 10.1038/nn.2220. [PubMed: 18849983]
29. Lin X, Patil S, Gao YG, and Qian A (2020). The Bone Extracellular Matrix in Bone Formation and Regeneration. Front Pharmacol 11, 757. 10.3389/fphar.2020.00757. [PubMed: 32528290]
30. Ortuño MJ, Susperregui AR, Artigas N, Rosa JL, and Ventura F (2013). Osterix induces Col1a1 gene expression through binding to Sp1 sites in the bone enhancer and proximal promoter regions. Bone 52, 548–556. 10.1016/j.bone.2012.11.007. [PubMed: 23159876]
31. Wang JS, Kamath T, Mazur CM, Mirzamohammadi F, Rotter D, Hojo H, Castro CD, Tokavanich N, Patel R, Govea N, et al. (2021). Control of osteocyte dendrite formation by Sp7 and its target gene osteocrin. Nat Commun 12, 6271. 10.1038/s41467-021-26571-7. [PubMed: 34725346]
32. Wu YF, Matsuo N, Sumiyoshi H, and Yoshioka H (2010). Sp7/Osterix is involved in the up-regulation of the mouse pro-α1(V) collagen gene (Col5a1) in osteoblastic cells. Matrix Biol 29, 701–706. 10.1016/j.matbio.2010.09.002. [PubMed: 20888414]
33. Yano H, Hamanaka R, Nakamura-Ota M, Adachi S, Zhang JJ, Matsuo N, and Yoshioka H (2014). Sp7/Osterix induces the mouse pro-α2(I) collagen gene (Col1a2) expression via the proximal promoter in osteoblastic cells. Biochem Biophys Res Commun 452, 531–536. 10.1016/j.bbrc.2014.08.100. [PubMed: 25172663]
34. Yun-Feng W, Matsuo N, Sumiyoshi H, and Yoshioka H (2010). Sp7/Osterix up-regulates the mouse pro-alpha3(V) collagen gene (Col5a3) during the osteoblast differentiation. Biochem Biophys Res Commun 394, 503–508. 10.1016/j.bbrc.2010.02.171. [PubMed: 20206127]
35. Shao X, Taha IN, Clauser KR, Gao YT, and Naba A (2020). MatrisomeDB: the ECM-protein knowledge database. Nucleic Acids Res 48, D1136–d1144. 10.1093/nar/gkz849. [PubMed: 31586405]

36. Gow A, Southwood CM, Li JS, Pariali M, Riordan GP, Brodie SE, Danias J, Bronstein JM, Kachar B, and Lazzarini RA (1999). CNS myelin and sertoli cell tight junction strands are absent in Osp/claudin-11 null mice. Cell 99, 649–659. 10.1016/s0092-8674(00)81553-6. [PubMed: 10612400]
37. Jarjour AA, Bull SJ, Almasieh M, Rajasekharan S, Baker KA, Mui J, Antel JP, Di Polo A, and Kennedy TE (2008). Maintenance of axo-oligodendroglial paranodal junctions requires DCC and netrin-1. J Neurosci 28, 11003–11014. 10.1523/jneurosci.3285-08.2008. [PubMed: 18945908]
38. Schaeren-Wiemers N, Bonnet A, Erb M, Erne B, Bartsch U, Kern F, Mantei N, Sherman D, and Suter U (2004). The raft-associated protein MAL is required for maintenance of proper axon--glia interactions in the central nervous system. J Cell Biol 166, 731–742. 10.1083/jcb.200406092. [PubMed: 15337780]
39. Traka M, Goutebroze L, Denisenko N, Bessa M, Nifli A, Havaki S, Iwakura Y, Fukamauchi F, Watanabe K, Soliven B, et al. (2003). Association of TAG-1 with Caspr2 is essential for the molecular organization of juxtaparanodal regions of myelinated fibers. J Cell Biol 162, 1161–1172. 10.1083/jcb.200305078. [PubMed: 12975355]
40. Yoshikawa F, Sato Y, Tohyama K, Akagi T, Hashikawa T, Nagakura-Takagi Y, Sekine Y, Morita N, Baba H, Suzuki Y, et al. (2008). Opalin, a transmembrane sialylglycoprotein located in the central nervous system myelin paranodal loop membrane. J Biol Chem 283, 20830–20840. 10.1074/jbc.M801314200. [PubMed: 18490449]
41. Bekku Y, Rauch U, Ninomiya Y, and Oohashi T (2009). Brevican distinctively assembles extracellular components at the large diameter nodes of Ranvier in the CNS. J Neurochem 108, 1266–1276. 10.1111/j.1471-4159.2009.05873.x. [PubMed: 19141078]
42. Dours-Zimmermann MT, Maurer K, Rauch U, Stoffel W, Fässler R, and Zimmermann DR (2009). Versican V2 assembles the extracellular matrix surrounding the nodes of ranvier in the CNS. J Neurosci 29, 7731–7742. 10.1523/jneurosci.4158-08.2009. [PubMed: 19535585]
43. Oohashi T, Hirakawa S, Bekku Y, Rauch U, Zimmermann DR, Su WD, Ohtsuka A, Murakami T, and Ninomiya Y (2002). Bral1, a brain-specific link protein, colocalizing with the versican V2 isoform at the nodes of Ranvier in developing and adult mouse central nervous systems. Mol Cell Neurosci 19, 43–57. 10.1006/mcne.2001.1061. [PubMed: 11817897]
44. Rasband MN, and Peles E (2021). Mechanisms of node of Ranvier assembly. Nat Rev Neurosci 22, 7–20. 10.1038/s41583-020-00406-8. [PubMed: 33239761]
45. Kaplan MR, Cho MH, Ullian EM, Isom LL, Levinson SR, and Barres BA (2001). Differential control of clustering of the sodium channels Na(v)1.2 and Na(v)1.6 at developing CNS nodes of Ranvier. Neuron 30, 105–119. 10.1016/s0896-6273(01)00266-5. [PubMed: 11343648]
46. Kaplan MR, Meyer-Franke A, Lambert S, Bennett V, Duncan ID, Levinson SR, and Barres BA (1997). Induction of sodium channel clustering by oligodendrocytes. Nature 386, 724–728. 10.1038/386724a0. [PubMed: 9109490]
47. Morawski M, Dityatev A, Hartlage-Rübsamen M, Blosa M, Holzer M, Flach K, Pavlica S, Dityateva G, Grosche J, Brückner G, and Schachner M (2014). Tenascin-R promotes assembly of the extracellular matrix of perineuronal nets via clustering of aggrecan. Philos Trans R Soc Lond B Biol Sci 369, 20140046. 10.1098/rstb.2014.0046. [PubMed: 25225104]
48. Eberle D, Fodelianaki G, Kurth T, Jagielska A, Möllmert S, Ulbricht E, Wagner K, Taubenberger AV, Träber N, and Escolano J-C (2020). Acquired demyelination but not genetic developmental defects in myelination leads to brain tissue stiffness changes. Brain Multiphysics 1, 100019.
49. Urbanski MM, Brendel MB, and Melendez-Vasquez CV (2019). Acute and chronic demyelinated CNS lesions exhibit opposite elastic properties. Sci Rep 9, 999. 10.1038/s41598-018-37745-7. [PubMed: 30700777]
50. Bertolio R, Napoletano F, Mano M, Maurer-Stroh S, Fantuz M, Zannini A, Bicciato S, Sorrentino G, and Del Sal G (2019). Sterol regulatory element binding protein 1 couples mechanical cues and lipid metabolism. Nat Commun 10, 1326. 10.1038/s41467-019-09152-7. [PubMed: 30902980]
51. Romani P, Brian I, Santinon G, Pocaterra A, Audano M, Pedretti S, Mathieu S, Forcato M, Bicciato S, Manneville JB, et al. (2019). Extracellular matrix mechanical cues regulate lipid metabolism through Lipin-1 and SREBP. Nat Cell Biol 21, 338–347. 10.1038/s41556-018-0270-5. [PubMed: 30718857]

52. Bentsen M, Goymann P, Schultheis H, Klee K, Petrova A, Wiegandt R, Fust A, Preussner J, Kuenne C, Braun T, et al. (2020). ATAC-seq footprinting unravels kinetics of transcription factor binding during zygotic genome activation. Nat Commun 11, 4267. 10.1038/s41467-020-18035-1. [PubMed: 32848148]
53. Lui JC, Raimann A, Hojo H, Dong L, Roschger P, Kikani B, Wintergerst U, Fratzl-Zelman N, Jee YH, Haeusler G, and Baron J (2022). A neomorphic variant in SP7 alters sequence specificity and causes a high-turnover bone disorder. Nat Commun 13, 700. 10.1038/s41467-022-28318-4. [PubMed: 35121733]
54. Dupree JL, Mason JL, Marcus JR, Stull M, Levinson R, Matsushima GK, and Popko B (2004). Oligodendrocytes assist in the maintenance of sodium channel clusters independent of the myelin sheath. Neuron Glia Biol 1, 179–192. 10.1017/s1740925×04000304. [PubMed: 18634596]
55. Djannatian M, Timmler S, Arends M, Luckner M, Weil MT, Alexopoulos I, Snaidero N, Schmid B, Misgeld T, Möbius W, et al. (2019). Two adhesive systems cooperatively regulate axon ensheathment and myelin growth in the CNS. Nat Commun 10, 4794. 10.1038/s41467-019-12789-z. [PubMed: 31641127]
56. Britsch S, Goerich DE, Riethmacher D, Peirano RI, Rossner M, Nave KA, Birchmeier C, and Wegner M (2001). The transcription factor Sox10 is a key regulator of peripheral glial development. Genes Dev 15, 66–78. 10.1101/gad.186601. [PubMed: 11156606]
57. Finzsch M, Schreiner S, Kichko T, Reeh P, Tamm ER, Bösl MR, Meijer D, and Wegner M (2010). Sox10 is required for Schwann cell identity and progression beyond the immature Schwann cell stage. J Cell Biol 189, 701–712. 10.1083/jcb.200912142. [PubMed: 20457761]
58. Stolt CC, Rehberg S, Ader M, Lommes P, Riethmacher D, Schachner M, Bartsch U, and Wegner M (2002). Terminal differentiation of myelin-forming oligodendrocytes depends on the transcription factor Sox10. Genes Dev 16, 165–170. 10.1101/gad.215802. [PubMed: 11799060]
59. Srinivasan R, Sun G, Keles S, Jones EA, Jang SW, Krueger C, Moran JJ, and Svaren J (2012). Genome-wide analysis of EGR2/SOX10 binding in myelinating peripheral nerve. Nucleic Acids Res 40, 6449–6460. 10.1093/nar/gks313. [PubMed: 22492709]
60. Saur AL, Fröb F, Weider M, and Wegner M (2021). Formation of the node of Ranvier by Schwann cells is under control of transcription factor Sox10. Glia 69, 1464–1477. 10.1002/glia.23973. [PubMed: 33566433]
61. Bekku Y, Su WD, Hirakawa S, Fässler R, Ohtsuka A, Kang JS, Sanders J, Murakami T, Ninomiya Y, and Oohashi T (2003). Molecular cloning of Bral2, a novel brain-specific link protein, and immunohistochemical colocalization with brevican in perineuronal nets. Mol Cell Neurosci 24, 148–159. 10.1016/s1044-7431(03)00133-7. [PubMed: 14550776]
62. Galtrey CM, Kwok JC, Carulli D, Rhodes KE, and Fawcett JW (2008). Distribution and synthesis of extracellular matrix proteoglycans, hyaluronan, link proteins and tenascin-R in the rat spinal cord. Eur J Neurosci 27, 1373–1390. 10.1111/j.1460-9568.2008.06108.x. [PubMed: 18364019]
63. Lemarchant S, Pruvost M, Montaner J, Emery E, Vivien D, Kanninen K, and Koistinaho J (2013). ADAMTS proteoglycanases in the physiological and pathological central nervous system. J Neuroinflammation 10, 133. 10.1186/1742-2094-10-133. [PubMed: 24176075]
64. Miyata S, and Kitagawa H (2016). Chondroitin 6-Sulfation Regulates Perineuronal Net Formation by Controlling the Stability of Aggrecan. Neural Plast 2016, 1305801. 10.1155/2016/1305801. [PubMed: 27057358]
65. Hume MA, Barrera LA, Gisselbrecht SS, and Bulyk ML (2015). UniPROBE, update 2015: new tools and content for the online database of protein-binding microarray data on protein-DNA interactions. Nucleic Acids Res 43, D117–122. 10.1093/nar/gku1045. [PubMed: 25378322]
66. Kadonaga JT, Jones KA, and Tjian R (1986). Promoter-specific activation of RNA polymerase II transcription by Sp1. Trends in Biochemical Sciences 11, 20–23.
67. Wang J, Zhuang J, Iyer S, Lin X, Whitfield TW, Greven MC, Pierce BG, Dong X, Kundaje A, Cheng Y, et al. (2012). Sequence features and chromatin structure around the genomic regions bound by 119 human transcription factors. Genome Res 22, 1798–1812. 10.1101/gr.139105.112. [PubMed: 22955990]

68. Wingender E, Schoeps T, and Dönitz J (2013). TFClass: an expandable hierarchical classification of human transcription factors. Nucleic Acids Res 41, D165–170. 10.1093/nar/gks1123. [PubMed: 23180794]
69. Zalc B (2016). The acquisition of myelin: An evolutionary perspective. Brain Res 1641, 4–10. 10.1016/j.brainres.2015.09.005. [PubMed: 26367449]
70. Zalc B, Goujet D, and Colman D (2008). The origin of the myelination program in vertebrates. Curr Biol 18, R511–512. 10.1016/j.cub.2008.04.010. [PubMed: 18579089]
71. Peter IS, and Davidson EH (2011). Evolution of gene regulatory networks controlling body plan development. Cell 144, 970–985. 10.1016/j.cell.2011.02.017. [PubMed: 21414487]
72. Peter IS, and Davidson EH (2016). Implications of Developmental Gene Regulatory Networks Inside and Outside Developmental Biology. Curr Top Dev Biol 117, 237–251. 10.1016/bs.ctdb.2015.12.014. [PubMed: 26969981]
73. Swift J, Ivanovska IL, Buxboim A, Harada T, Dingal PC, Pinter J, Pajerowski JD, Spinler KR, Shin JW, Tewari M, et al. (2013). Nuclear lamin-A scales with tissue stiffness and enhances matrix-directed differentiation. Science 341, 1240104. 10.1126/science.1240104. [PubMed: 23990565]
74. Malavasi EL, Ghosh A, Booth DG, Zagnoni M, Sherman DL, and Brophy PJ (2021). Dynamic early clusters of nodal proteins contribute to node of Ranvier assembly during myelination of peripheral neurons. Elife 10. 10.7554/eLife.68089.
75. Wheeler NA, and Fuss B (2016). Extracellular cues influencing oligodendrocyte differentiation and (re)myelination. Exp Neurol 283, 512–530. 10.1016/j.expneurol.2016.03.019. [PubMed: 27016069]
76. Macchi M, Magalon K, Zimmer C, Peeva E, El Waly B, Brousse B, Jaekel S, Grobe K, Kiefer F, Williams A, et al. (2020). Mature oligodendrocytes bordering lesions limit demyelination and favor myelin repair via heparan sulfate production. Elife 9. 10.7554/eLife.51735.
77. Zhou T, Gao B, Fan Y, Liu Y, Feng S, Cong Q, Zhang X, Zhou Y, Yadav PS, Lin J, et al. (2020). Piezo1/2 mediate mechanotransduction essential for bone formation through concerted activation of NFAT-YAP1-ß-catenin. Elife 9. 10.7554/eLife.52779.
78. Dugas JC, Ibrahim A, and Barres BA (2012). The T3-induced gene KLF9 regulates oligodendrocyte differentiation and myelin regeneration. Mol Cell Neurosci 50, 45–57. 10.1016/j.mcn.2012.03.007. [PubMed: 22472204]
79. Torvund-Jensen J, Steengaard J, Reimer L, Fihl LB, and Laursen LS (2014). Transport and translation of MBP mRNA is regulated differently by distinct hnRNP proteins. J Cell Sci 127, 1550–1564. 10.1242/jcs.140855. [PubMed: 24522184]
80. Elbaz B, Yang L, Vardy M, Isaac S, Rader BL, Kawaguchi R, Traka M, Woolf CJ, Renthal W, and Popko B (2022). Sensory neurons display cell-type-specific vulnerability to loss of neuron-glia interactions. Cell Rep 40, 111130. 10.1016/j.celrep.2022.111130. [PubMed: 35858549]
81. Gao X, Gillig TA, Ye P, D'Ercole AJ, Matsushima GK, and Popko B (2000). Interferon-gamma protects against cuprizone-induced demyelination. Mol Cell Neurosci 16, 338–349. 10.1006/mcne.2000.0883. [PubMed: 11085872]
82. Elbaz B, Traka M, Kunjamma RB, Dukala D, Brosius Lutz A, Anton ES, Barres BA, Soliven B, and Popko B (2016). Adenomatous polyposis coli regulates radial axonal sorting and myelination in the PNS. Development 143, 2356–2366. 10.1242/dev.135913. [PubMed: 27226321]
83. Traka M, Millen KJ, Collins D, Elbaz B, Kidd GJ, Gomez CM, and Popko B (2013). WDR81 is necessary for purkinje and photoreceptor cell survival. J Neurosci 33, 6834–6844. 10.1523/jneurosci.2394-12.2013. [PubMed: 23595742]
84. Xu H, Dzhashiashvili Y, Shah A, Kunjamma RB, Weng YL, Elbaz B, Fei Q, Jones JS, Li YI, Zhuang X, et al. (2020). m(6)A mRNA Methylation Is Essential for Oligodendrocyte Maturation and CNS Myelination. Neuron 105, 293–309.e295. 10.1016/j.neuron.2019.12.013. [PubMed: 31901304]
85. Auer RN (1994). Automated nerve fibre size and myelin sheath measurement using microcomputer-based digital image analysis: theory, method and results. J Neurosci Methods 51, 229–238. 10.1016/0165-0270(94)90015-9. [PubMed: 8051953]

86. Elbaz B, Aaker JD, Isaac S, Kolarzyk A, Brugarolas P, Eden A, and Popko B (2018). Phosphorylation State of ZFP24 Controls Oligodendrocyte Differentiation. Cell Rep 23, 2254–2263. 10.1016/j.celrep.2018.04.089. [PubMed: 29791837]

87. Emery B, and Dugas JC (2013). Purification of oligodendrocyte lineage cells from mouse cortices by immunopanning. Cold Spring Harb Protoc 20l3, 854–868. 10.1101/pdb.prot073973.

88. Maneshi MM, Toth AB, Ishii T, Hori K, Tsujikawa S, Shum AK, Shrestha N, Yamashita M, Miller RJ, Radulovic J, et al. (2020). Orai1 Channels Are Essential for Amplification of Glutamate-Evoked Ca(2+) Signals in Dendritic Spines to Regulate Working and Associative Memory. Cell Rep 33, 108464. 10.1016/j.celrep.2020.108464. [PubMed: 33264616]

89. Dobin A, Davis CA, Schlesinger F, Drenkow J, Zaleski C, Jha S, Batut P, Chaisson M, and Gingeras TR (2013). STAR: ultrafast universal RNA-seq aligner. Bioinformatics 29, 15–21. 10.1093/bioinformatics/bts635. [PubMed: 23104886]

90. Li H, Handsaker B, Wysoker A, Fennell T, Ruan J, Homer N, Marth G, Abecasis G, and Durbin R (2009). The Sequence Alignment/Map format and SAMtools. Bioinformatics 25, 2078–2079. 10.1093/bioinformatics/btp352. [PubMed: 19505943]

91. Liao Y, Smyth GK, and Shi W (2014). featureCounts: an efficient general purpose program for assigning sequence reads to genomic features. Bioinformatics 30, 923–930. 10.1093/bioinformatics/btt656. [PubMed: 24227677]

92. Love MI, Huber W, and Anders S (2014). Moderated estimation of fold change and dispersion for RNA-seq data with DESeq2. Genome Biol 15, 550. 10.1186/s13059-014-0550-8. [PubMed: 25516281]

93. Blecher-Gonen R, Barnett-Itzhaki Z, Jaitin D, Amann-Zalcenstein D, Lara-Astiaso D, and Amit I (2013). High-throughput chromatin immunoprecipitation for genome-wide mapping of in vivo protein-DNA interactions and epigenomic states. Nat Protoc 8, 539–554. 10.1038/nprot.2013.023. [PubMed: 23429716]

94. Kofler R, Langmüller AM, Nouhaud P, Otte KA, and Schlötterer C (2016). Suitability of Different Mapping Algorithms for Genome-Wide Polymorphism Scans with Pool-Seq Data. G3 (Bethesda) 6, 3507–3515. 10.1534/g3.116.034488. [PubMed: 27613752]

95. Heinz S, Benner C, Spann N, Bertolino E, Lin YC, Laslo P, Cheng JX, Murre C, Singh H, and Glass CK (2010). Simple combinations of lineage-determining transcription factors prime cis-regulatory elements required for macrophage and B cell identities. Mol Cell 38, 576–589. 10.1016/j.molcel.2010.05.004. [PubMed: 20513432]

96. Machanick P, and Bailey TL (2011). MEME-ChIP: motif analysis of large DNA datasets. Bioinformatics 27, 1696–1697. 10.1093/bioinformatics/btr189. [PubMed: 21486936]

97. McLean CY, Bristor D, Hiller M, Clarke SL, Schaar BT, Lowe CB, Wenger AM, and Bejerano G (2010). GREAT improves functional interpretation of cis-regulatory regions. Nat Biotechnol 28, 495–501. 10.1038/nbt.1630. [PubMed: 20436461]

98. Lawrence M, Huber W, Pagès H, Aboyoun P, Carlson M, Gentleman R, Morgan MT, and Carey VJ (2013). Software for computing and annotating genomic ranges. PLoS Comput Biol 9, e1003118. 10.1371/journal.pcbi.1003118. [PubMed: 23950696]

99. Langmead B, and Salzberg SL (2012). Fast gapped-read alignment with Bowtie 2. Nat Methods 9, 357–359. 10.1038/nmeth.1923. [PubMed: 22388286]

100. Ramírez F, Dündar F, Diehl S, Grüning BA, and Manke T (2014). deepTools: a flexible platform for exploring deep-sequencing data. Nucleic Acids Res 42, W187–191. 10.1093/nar/gku365. [PubMed: 24799436]

101. Feng J, Liu T, Qin B, Zhang Y, and Liu XS (2012). Identifying ChIP-seq enrichment using MACS. Nat Protoc 7, 1728–1740. 10.1038/nprot.2012.101. [PubMed: 22936215]

102. Khan A, Fornes O, Stigliani A, Gheorghe M, Castro-Mondragon JA, van der Lee R, Bessy A, Chèneby J, Kulkarni SR, Tan G, et al. (2018). JASPAR 2018: update of the open-access database of transcription factor binding profiles and its web framework. Nucleic Acids Res 46, D1284. 10.1093/nar/gkx1188. [PubMed: 29161433]

103. Kulakovskiy IV, Vorontsov IE, Yevshin IS, Sharipov RN, Fedorova AD, Rumynskiy EI, Medvedeva YA, Magana-Mora A, Bajic VB, Papatsenko DA, et al. (2018). HOCOMOCO: towards a complete collection of transcription factor binding models for human and mouse

via large-scale ChIP-Seq analysis. Nucleic Acids Res 46, D252–d259. 10.1093/nar/gkx1106. [PubMed: 29140464]

104. Ikai A, Afrin R, Sekiguchi H, Okajima T, Alam MT, and Nishida S (2003). Nano-mechanical methods in biochemistry using atomic force microscopy. Curr Protein Pept Sci 4, 181–193. 10.2174/1389203033487171. [PubMed: 12769717]

Highlights

Each highlight can be no more than 89 characters, including spaces.

1. Osterix (Sp7) is required for developmental myelination and node of Raniver formation.
2. In adults, Osterix is important for myelin maintenance and for remyelination.
3. Osterix regulates ECM and node of Ranvier-related gene expression in oligodendrocytes.
4. Sp7 changes Sox10 DNA binding to enhancers of ECM and node of Ranvier-related genes.

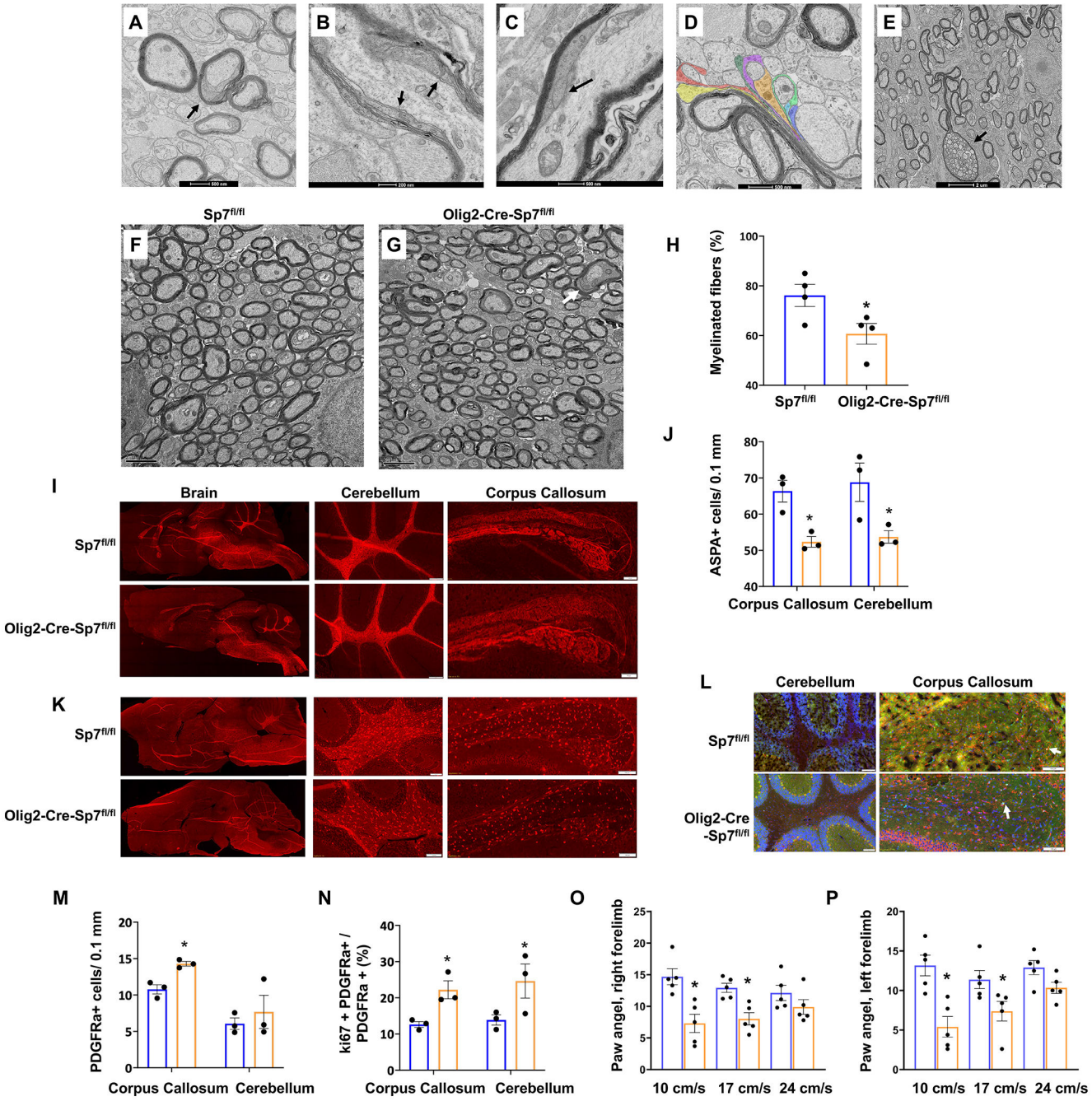

Figure 1. Sp7 is required for normal developmental myelination.

(A-E) P15 Sp7$^{fl/fl}$;Olig2-Cre optic nerves were examined by EM. The following paranodal and juxtparanodal abnormalities were observed in the mutant: (A) abnormal loops of non-compact myelin below compact internodal myelin, (B-C) non-compact myelin inside (B) and below (C) compact myelin, and (D) non-compact myelin loops, originating from the compact myelin sheets, (E) axonal swelling with accumulation of organelles. (F-G) Optic nerves of 21-days-old Sp7$^{fl/fl}$;Olig2-Cre mice were examined by EM. White arrow denotes growth of non-compact myelin beneath compact myelin. (H) Reduced percentage

of myelinated fibers in the mutant. (I-K) Brains of P21 $Sp7^{fl/fl}$;Olig2-Cre mice and control $Sp7^{fl/fl}$ mice were analyzed by IHC with antibodies against MBP (I) and ASPA (K). (J) Quantified results. Blue bar-WT, orange bar-mutant. (L) Brains of P21 $Sp7^{fl/fl}$;Olig2-Cre mice and control $Sp7^{fl/fl}$ mice were analyzed by IHC with antibodies against PDGFRα (red) and Ki67 (green). (M-N) Quantified results. Blue bars-WT, orange bars-mutant. (O-P) Gait analysis was performed on 3-month-old $Sp7^{fl/fl}$;Olig2-Cre mice and control $Sp7^{fl/fl}$ male mice. (O) Paw angel, right forelimb. (P) Paw angel, left hindlimb. For panels A-E, n=3 for WT and mutant. For panels F-H n=4 for WT and mutant. For panels I-N n=3 for WT and mutant. For gait analysis, n=5 males per genotype. *P<0.05 (two-tailed unpaired Student's t-test). Data are presented as the mean ± SEM. Scale bars in A=500 nm, B=200 nm, C=500 nm, D=500 nm, E, F and G= 2 μm, I and L= 100 μm.

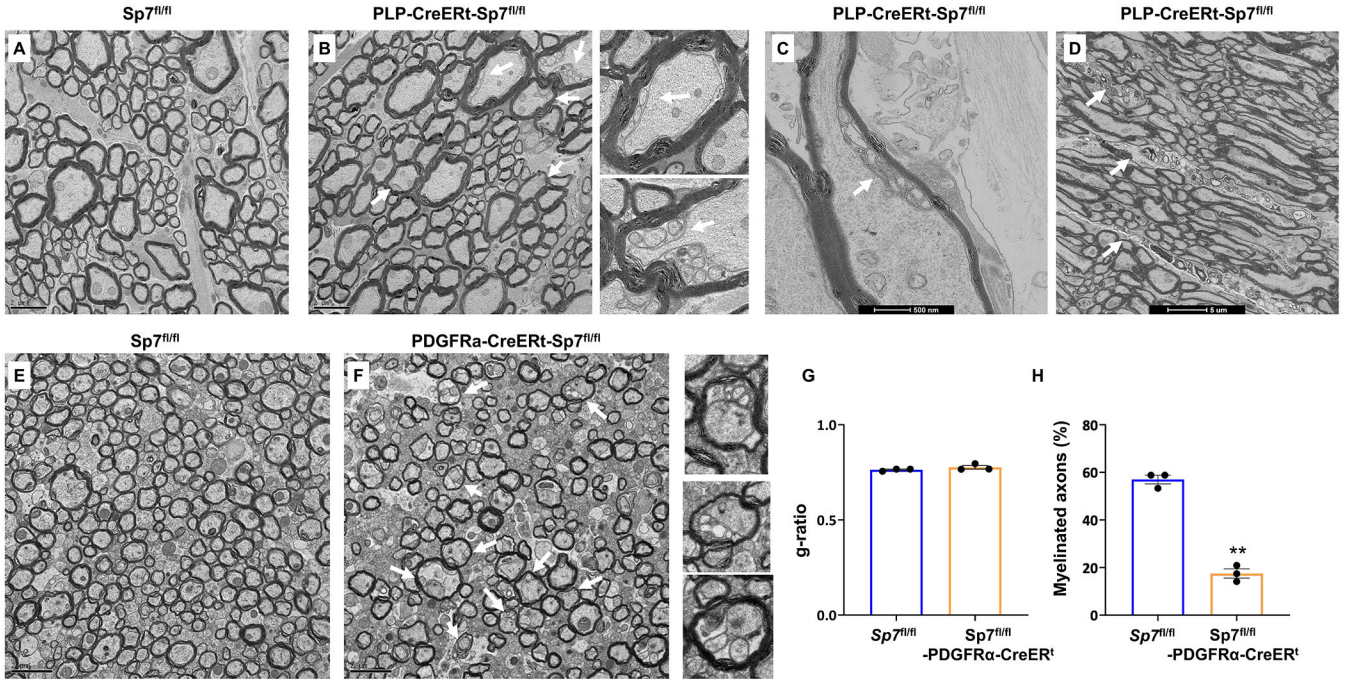

Figure 2. Sp7 is important for myelin maintenance and remyelination in adult mice.

Two-months-old $Sp7^{fl/fl}$;PLP-$CreER^t$ mice and control $Sp7^{fl/fl}$ mice were injected with tamoxifen for five consecutive days. Three months post-injection optic nerves were analyzed by EM. (A) Optic nerves of WT mice were intact. (B-C) Growth of non-compact myelin was observed in the mutant beneath compact myelin in cross (B) and longitudinal (C) sections. (D) Phagocytic cells with myelin debris were observed in the mutants. (E-H) $Sp7^{fl/fl}$-PDGFRα-$CreER^t$ mice and control $Sp7^{fl/fl}$ mice were injected with tamoxifen for five consecutive days. Two weeks post-injection, mice were fed cuprizone chow for six weeks to induce demyelination. After six weeks, mice were fed normal chow for three weeks to allow remyelination. Following the remyelination period, the corpus callosum was analyzed by EM. (E-F) Reduced numbers of myelinated fibers were observed in the corpus callosum of the Sp-7 ablated mice. Higher magnification: non compact myelin loops were present in the mutant beneath compact internodal myelin. (G) Myelin thickness (g-ratio) was similar between WT and mutant upon remyelination. (H) Reduced percentage of myelinated fibers in $Sp7^{fl/fl}$-PDGFRα-$CreER^t$ mice. For A-D and for E-F, n=3 for WT and mutant. **P<0.01 (two-tailed unpaired Student's t-test). Data are presented as mean ± SEM. Scale bars in A and B=2 μm, C=500 nm, D=5 μm, E and F = 2 μm.

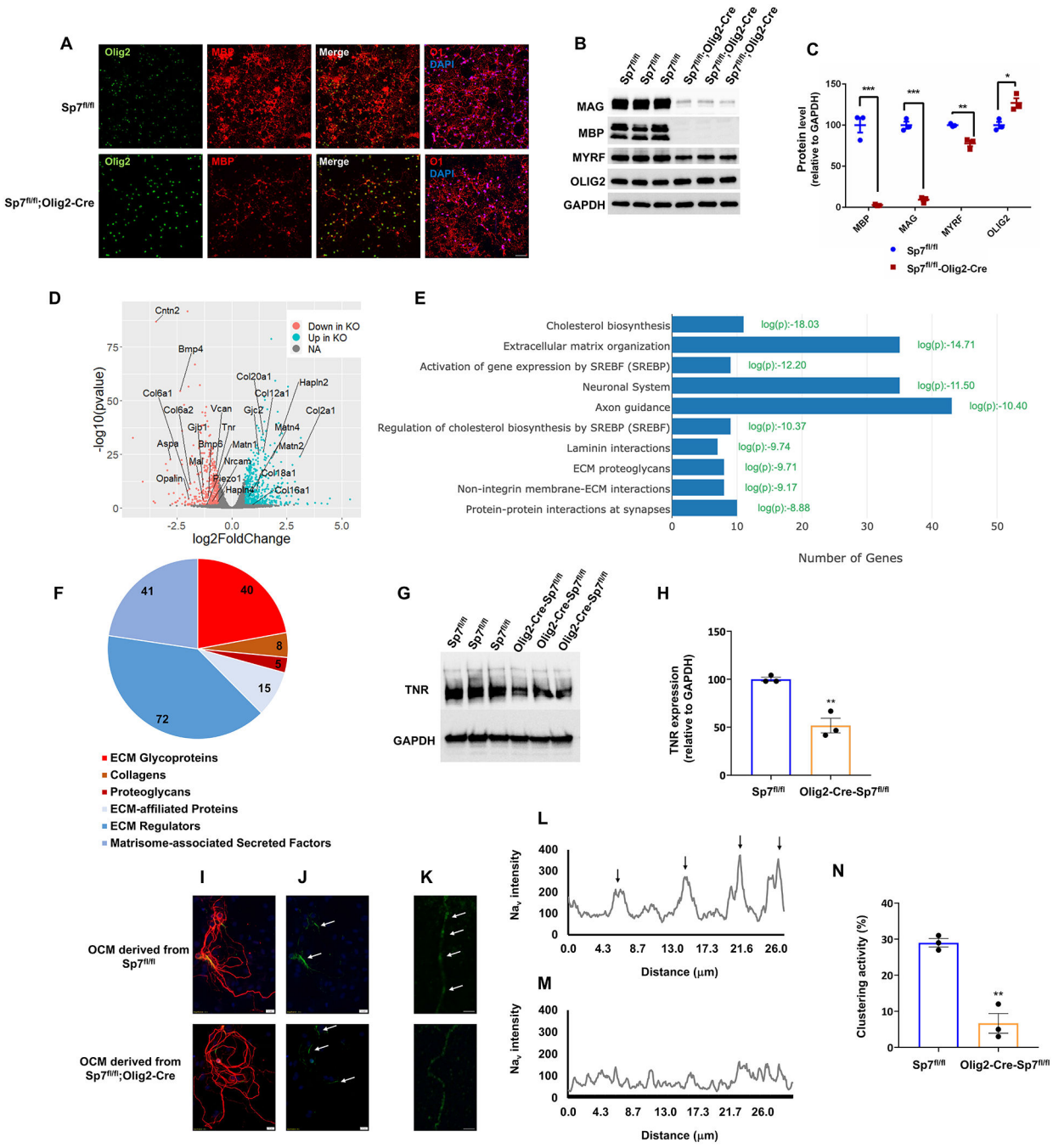

Figure 3. Sp7 controls the expression of genes involved in node of Ranvier and ECM formation.

Primary OPCs were isolated from 6-days-old (P6) $Sp7^{fl/fl}$;Olig2-Cre and $Sp7^{fl/fl}$ mice (used as controls) using the antibody-panning approach. Cells were allowed to differentiate for five days before harvesting for RNA and protein isolation. (A) Reduced MBP staining in primary cultured oligodendrocytes derived from the $Sp7^{fl/fl}$;Olig2-Cre mice. Cells were stained with antibodies against Olig2 (green), MBP (red) and O4 (purple). (B) Protein extracts were subjected to Western blots with the indicated antibodies. (C) Quantified results. (D) Volcano plot of differently expressed genes in Sp7 ablated cells (RNA-seq). (E). GO analysis of

differentially expressed transcript in Sp7-ablated oligodendrocytes. (F) Matrisome genes in differentially expressed transcripts. Red-brown represents core matrisome genes, and blue represent matrisome-associated transcripts. (G) Validation of RNA-seq results by WB. Protein lysates from brains of 21-days-old $Sp7^{fl/fl}$;Olig2-Cre and $Sp7^{fl/fl}$ mice were used. (H) Quantified results of Western blot; protein expression relative to GAPDH. (I-N) OCM derived from *Sp7*-ablated oligodendrocytes has reduced sodium channel clustering activity: Primary oligodendrocytes derived from $Sp7^{fl/fl}$;Olig2-Cre or $Sp7^{fl/fl}$ mice (used as controls) were cultured, and OCM collected. In parallel, primary hippocampal neurons were isolated from neonatal mice. At DIV 3, OCM derived from $Sp7^{fl/fl}$;Olig2-Cre or $Sp7^{fl/fl}$ mice was added to cultured hippocampal neurons. Clustering activity was determined at DIV 21. (I) Neurites were stained with an antibodies against neurofilament M (NFM; red) and sodium channels (green). (J) Axon initial segments (AIS) were detected (white arrow) in all hippocampal neurons grown with either OCM derived from $Sp7^{fl/fl}$;Olig2-Cre or $Sp7^{fl/fl}$ cells. \ (K) To study sodium channel clustering, Z-series of optical sections were collected from axons at 0.3 μm increments, and sodium channel immunofluorescence intensity was analyzed at maximum orthogonal projection. Sodium channel clusters are marked by white arrows. (L and M). Fluorescence intensity profiles corresponding to axonal sodium channel staining from panel K. Individual peaks that represent sodium channel clusters are marked by black arrow. (N) Oligodendrocyte-specific ablation of *Sp7* reduces sodium channel clustering activity in hippocampal neurons. Clustering activity represents the percentage of axons of cultured hippocampal neurons having at least two sodium channel clusters at 21 DIV. In panels I-N, sodium channel clusters were defined by sodium channel labeling intensity that is ≥2.5-fold over the basal level along the axon. Axons were identified by the presence of AIS. Scale bar in panel A =100 μm, in panels I-K= 20 μm. For panels A-C n=3 for Wt and mutant. For RNA-seq in D-F n=2 for WT and mutant. For panels G-H n=3 for WT and mutant. For panels I-N, at least 115 hippocampal neurons were analyzed per condition. *P< 0.05, **P<0.01 , ***P<0.001 (two-tailed unpaired Student’s t-test). Data are presented as mean ± SEM.

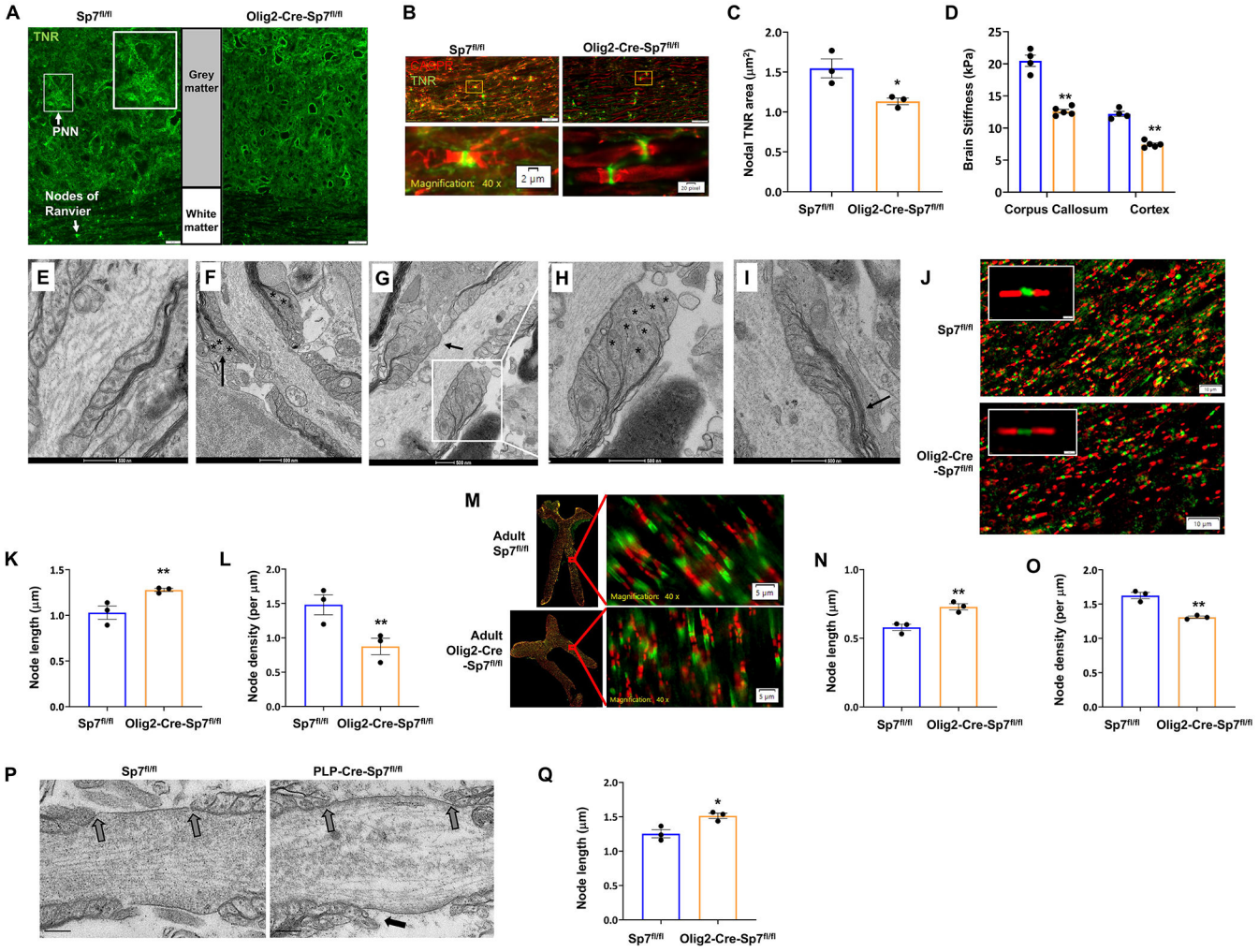

Figure 4. Sp7 is crucial for node of Ranvier integrity and brain stiffness.

(A-B) Longitudinal sections of lumbar spinal cord of $Sp7^{fl/fl}$;Olig2-Cre and $Sp7^{fl/fl}$ mice (used as controls) were analyzed by IHC using TNR (green) and CASPR (red) antibodies. In grey matter, TNR staining was observed in perineuronal nets (PNN) (insertion to A) and in white matter, TNR staining was observed in nodes of Ranvier. (B) TNR stanning in node (green), marked by CASPR (red). (C) quantified TNR stanning in nodes. TNR stanning flanked by two CASRP stanning were used for quantification. (D) Brain stiffness $Sp7^{fl/fl}$;Olig2-Cre and $Sp7^{fl/fl}$ mice (used as controls). Blue bars-WT, orange bars-mutant. (E-I) Nodes of Ranvier were examined by EM in optic nerves of P15 mice. (E) Normal paranodal area in $Sp7^{fl/fl}$ mice. (F and G) Splits in compact myelin at the paranode area were observed in $Sp7^{fl/fl}$;Olig2-Cre mice, where paranodal loops were growing between compact myelin layers (black arrow). White rectangle denotes enlarged area in H. (H) Paranodal loops not in contact with axolemma were observed in the mutants (black asterisks). (I) areas of non-compact myelin between two layers of compact myelin were observed in the mutant (black arrow). (J-L) Coronal sections of 21-days-old $Sp7^{fl/fl}$;Olig2-Cre and $Sp7^{fl/fl}$ mice were stained with anti-CASPR antibodies (red, paranodal) and anti-sodium channel antibodies (green, nodal) and nodes of Ranvier in the corpus callosum were

analyzed. Insertion to J: an example of nodes that were analyzed. (K-L) Quantified results. Full nodes that have nodal sodium channel staining (green) engulfed by two CASPR domains (red) were quantified. (M-O) Longitudinal optic nerve sections of three-months-old $Sp7^{fl/fl}$;Olig2-Cre and $Sp7^{fl/fl}$ mice were stained with CASPR (red, paranodal) and potassium channel (green, juxtaparanodal). (N-O) Quantified results. (P-O) Two-months-old $Sp7^{fl/fl}$;PLP-$CreER^t$ mice and control $Sp7^{fl/fl}$ mice were injected with tamoxifen for five consecutive days. Three months post-injection ultrathin longitudinal sections of spinal cord were analyzed by EM. (O) Abnormally long nodal gaps in mutant (nodal boundaries are indicated by black arrows). Abnormal paranodal loops oriented away from axolemma are indicated by black arrows. (P) Quantified results. For panels A-C, n=3 for WT and mutant. For TNR quantification over 50 nodes per mouse were quantified, from three different mice per genotype. For EM in panels E-I, n=2 for WT and 3 for mutant. For IHC in panel J-L, n=3 for WT and mutant, over 400 nodes were quantified per each genotype. Nodal length in panels K and N represents the distance between two paranodes (flanked by CASPR). Only nodes with clear CASPR staining on both sides were quantified. For P-O, a minimum of 10 nodal regions were imaged per mouse to quantify node of Ranvier length, from three different mice per genotype. *P< 0.05, **P<0.01. (Two-tailed unpaired Student's t-test). Data are presented as mean ± SEM. Scale bars in A=20 μm (left) and 50 μm (right), B=2 μm, E-I=500 nm, J=10 μm, and M= 5 μm.

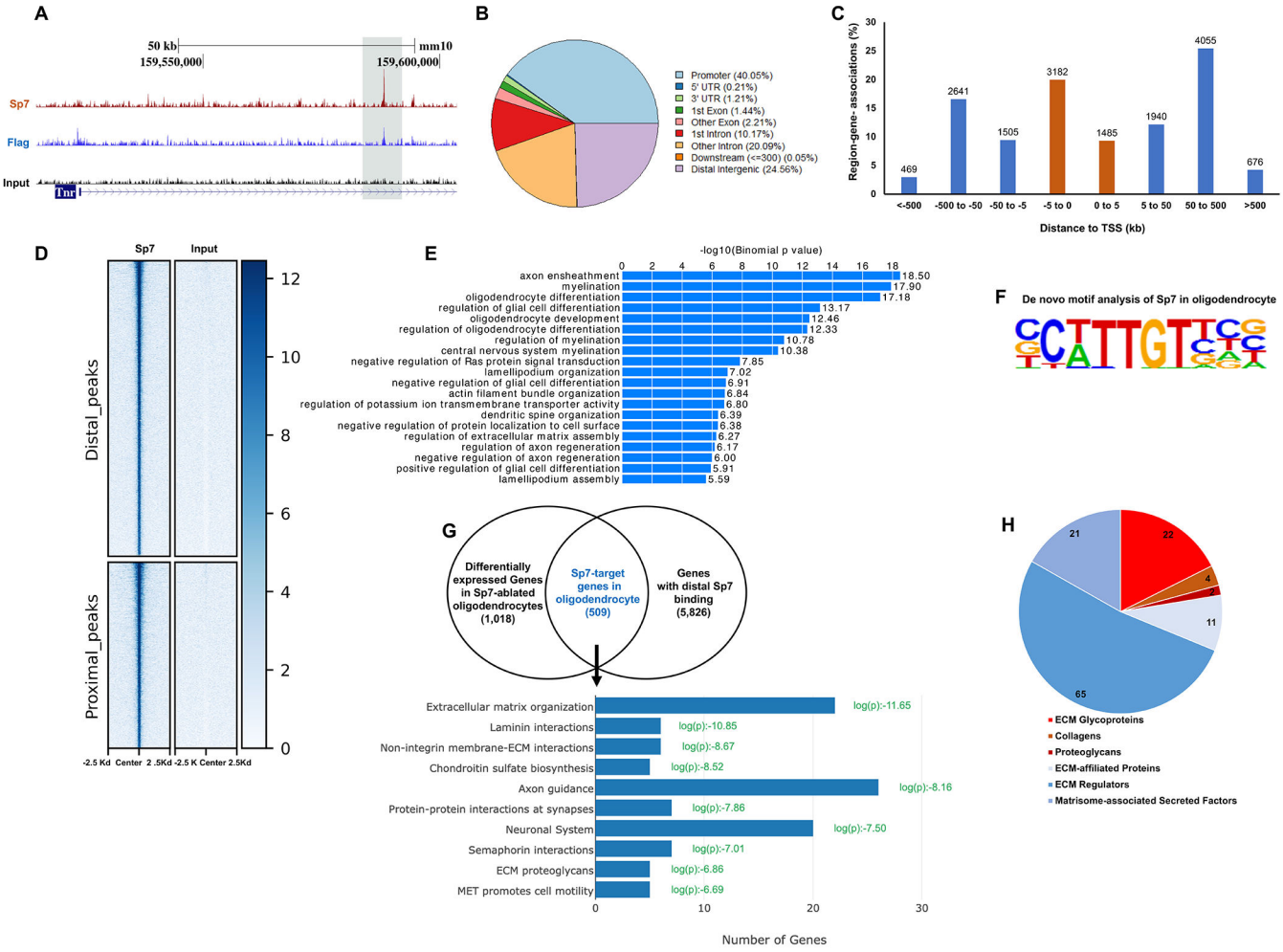

Figure 5. Sp7 enhancers in oligodendrocyte lineage cells.

Sp7 ChIP-seq was performed on primary cultured oligodendrocytes. (A) an example of Sp7 binding in the first intron of *Tnr*, showing Sp7 signal intensity as identified using anti-Sp7 antibody (orange) and anti-Flag antibody (blue). (B) Genomic distribution of oligodendrocyte-specific Sp7-binding sites. (C) Sp7 peaks were classified as proximal (orange) or distal (blue) to transcription start site (TSS). (D) Oligodendrocyte-specific Sp7-bound peaks. (E) Gene ontology analysis of genes linked to oligodendrocyte specific distal Sp7 peaks. (F) De-novo analysis of oligodendrocyte-specific Sp7 peaks identified Sox binding sites as the most enriched among Sp7 peaks, p=1e-947. (G) Gene ontology analysis of Sp7 target genes in oligodendrocytes. (H) Matrisome genes in Sp7-target genes. Red-brown represents core matrisome genes, and blues represent matrisome associated transcripts. For the Chip-seq studies in A-D, n=2 for Sp7 Chip-seq and for input DNA.

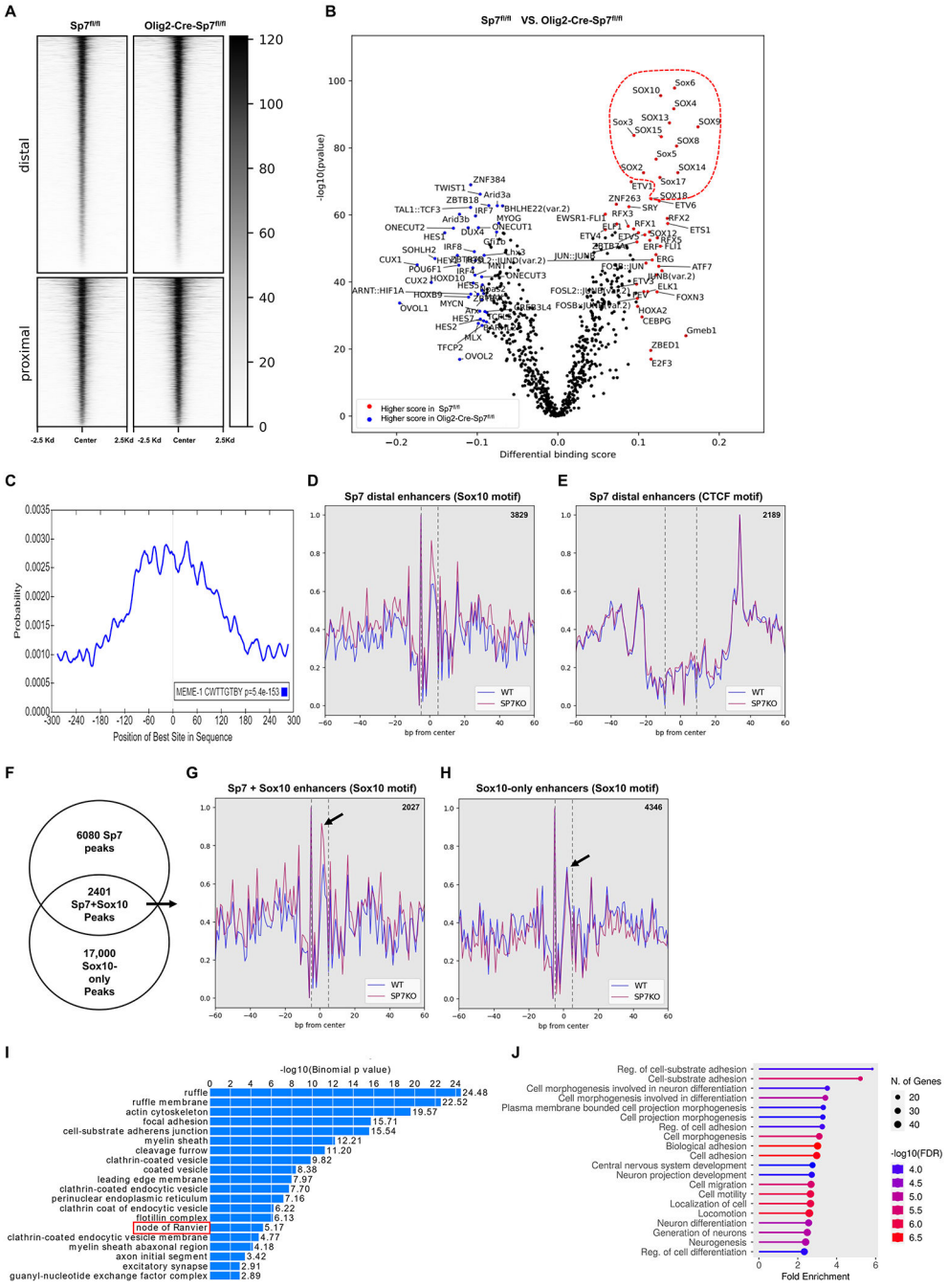

Figure 6. Sp7 acts in open chromatin, where it changes Sox10 binding.

(A) ATAC-seq normalized signal in Sp7 bound peaks in mature oligodendrocyte. Each row represents the location of Sp7 binding in oligodendrocyte (Same sites as in fig 5D). Signal intensity resemble ATAC-seq signal in this site.(B) Differential footprinting analysis, based on normalized, corrected ATAC-seq signal comparing transcription factor binding between oligodendrocyte derived from $Sp7^{fl/fl}$;Olig2-Cre and $Sp7^{fl/fl}$ mice. Sox transcription factor with similar binding motif that had higher binding score in the oligodendrocytes derived from $Sp7^{fl/fl}$ mice are marked in dashed red line. Sp7 ablation substantially reduced Sox10

binding to Sp7 distal enhancers with differential binding score=0.13, Pval=2.45E-96. (C) Central localization of Sox10 motif in oligodendrocyte-specific Sp7-bound distal peaks. (D) Aggregated normalized ATAC signal around transcription factor Sox10 motif (marked by dashed lines) in distal Sp7 peaks. (E) Aggregated normalized ATAC signal around transcription factor CTCF motif (marked by dashed lines) in distal Sp7 peaks. Note differential accessibility in Sox10 motifs but not in CTCF motifs found in the same set of distal ATAC peaks. (F) Intersection of distal Sp7 ChIP-called peaks (same as Fig 5) with Sox10 ChIP-called peaks[20] was used to select sites for further investigation. (G) Aggregated normalized ATAC-seq signal at Sox10 motif in distal Sp7 peaks that were also bound with Sox10. (H) Aggregated footprint signal of transcription factor Sox10 in peaks that were devoid of Sp7. Note differential accessibility in Sox10 motifs in Sp7 and Sox10 peaks, but not in Sox10 positive, Sp7 negative peaks. (I) Gene ontology (GREAT) analysis of genes associated with regions with Sp7 and Sox10 overlapping ChIP called peaks. Red rectangle denotes the GO term “node of Ranvier”. (J) Shiny GO analysis of genes found near Sp7 and Sox10 overlapping peaks and also differentially expressed upon ablation of Sp7 in oligodendrocytes. In panels D, E, G and H blue line represents ATAC signal in Cre negative $Sp7^{fl/fl}$ mice and red line represents ATAC signal in $Sp7^{fl/fl}$;Olig2-Cre mice.

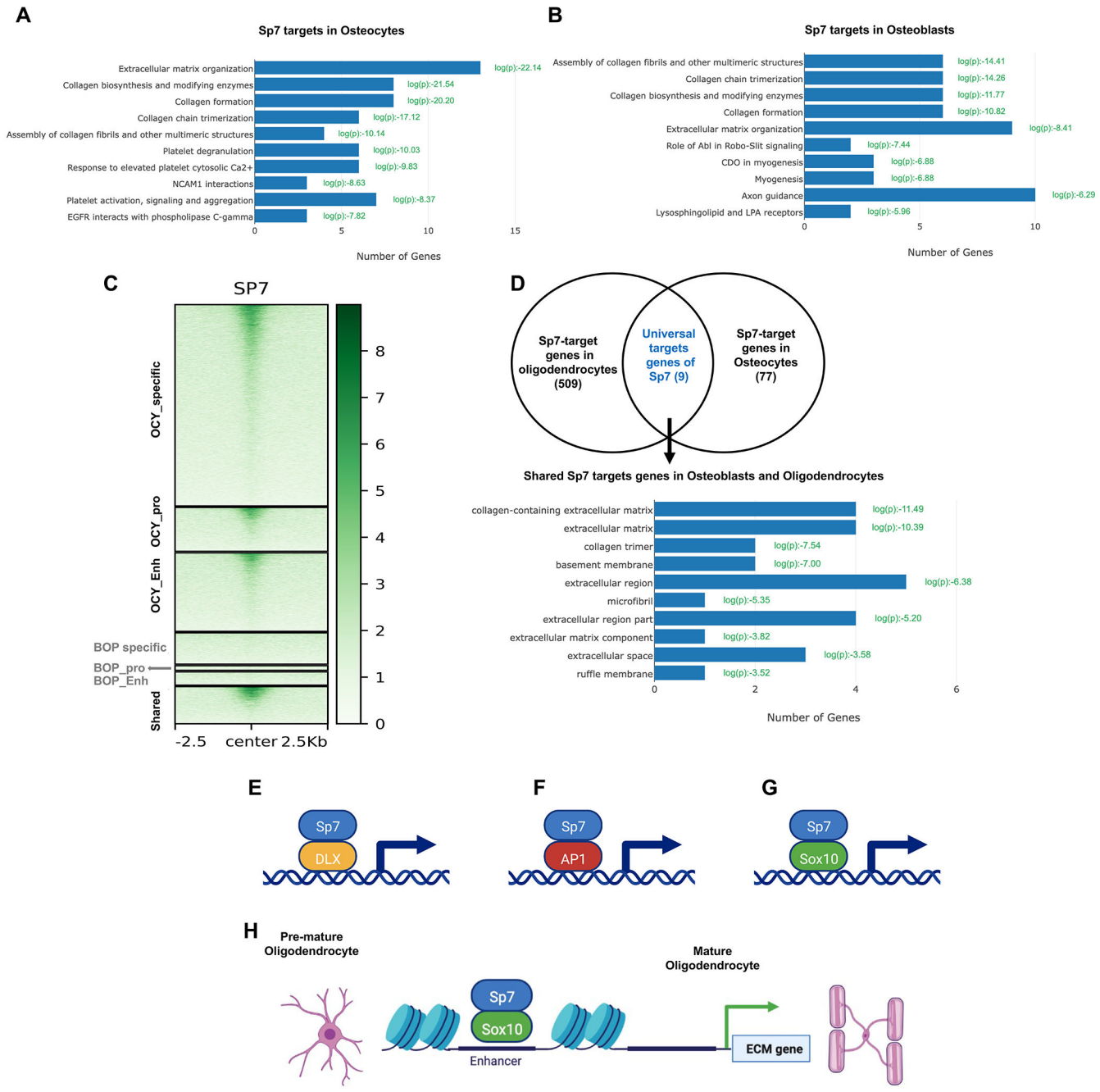

Figure 7. Convergent and divergent biological activity of Sp7 in the CNS and in bones.

(A) Gene ontology (Reactom) analysis of Sp7-target genes in osteocytes. (B) Gene ontology (Reactom) analysis of Sp7-target genes in osteoblasts. (C) Heatmap showing Sp7 ChIP signal from oligodendrocytes in regions found to bind Sp7 in bone lineage cells. Each row represents the location of Sp7 binding in bone lineage. Rows are grouped based on Sp7 binding in osteocytes (Ocy) or osteoblasts (POB) separated to proximal peaks (Pro) and distal enhancers (Enh)[31]. POB-specific Sp7 sites were generally not Sp7 bound in oligodendrocytes, but many osteocyte-specific Sp7 binding sites and some shared POB and

Ocy enhancers also bind Sp7 in oligodendrocytes. (D) Gene ontology (Reactom) analysis of Sp7-target genes shared in both osteocytes and oligodendrocyte. (E-H) Our model of Sp7 activity in CNS and in bones. (E) Sp7 acts with DLX proteins in osteoblasts. (F) As osteoblasts transition to osteocytes, Sp7 changes its cofactor to AP1 members (FOS;JUN) in osteocytes. (G) Sp7 acts with Sox10 in oligodendrocytes. (H) During oligodendrocyte differentiation, Sp7 mediates Sox10 binding to DNA in distal enhancers of ECM related genes and mediates their expression.

Key resources table

REAGENT or RESOURCE	SOURCE	IDENTIFIER
Antibodies		
Mouse anti-TNR	R and D Systems	cat #MAB1624 RRID:AB_2207001
Rabbit-anti-MBP	Abcam	Cat# ab40390 RRID:AB_1141521
Rabbit anti ASPA	Genetex	Cat # AB15580 RRID:AB_443209
Rabbit anti IBA1	Wako Pure Chemical	Cat # 019–19741 RRID:AB_839504
Rabbit anti-parvalbumin	Swant	Cat# PV27, RRID:AB_2631173
Mouse anti Kv1.2 K+ channel	Antibodies Incorporated	Cat# 75-008, RRID:AB_2296313
Rabbit anit Sp7	Abcam	Cat# ab22552, RRID:AB_2194492)
Mouse anti Flag	Sigma-Aldrich	Cat# F1804, RRID:AB_262044
Goat anti-PDGFR-α	R&D Systems	Cat# AF1062; RRID: AB_2236897
Rabbit anti-MBP	Abcam	Cat# ab40390; RRID: AB_1141521
Mouse anti-CC1	Millipore	Cat# OP80; RRID: AB_2057371
Mouse anti-Olig2	Millipore	Cat# MABN50; RRID: AB_10807410
Mouse anti-O1	R&D Systems	Cat# MAB1327; RRID: AB_357618
Rabbit anti-Ki67	Abcam	Cat# AB15580; RRID: AB_805388
Rabbit anti-MAG	Thermo Fisher Scientific	Cat# 34-6200, RRID: AB_2533179
Mouse anti-MBP	BioLegend	Cat# SMI 99; RRID: AB_2314771
Mouse anti-MYRF	Kindly provided by Dr. Ben Emery	Cat# 4G4; RRID: AB_2814997
Mouse anti-GAPDH	Cell Signaling	Cat# 2118; RRID: AB_561053
Rabbit anti-Caspr	Abcam	Cat# ab34151; RRID: AB_869934
Mouse anti-Sodium channel, pan	Sigma-Aldrich	Cat# S8809; RRID: AB_477552
Rabbit anti Neurofilament M	Millipore	Cat# AB1987, RRID:AB_91201
Bacterial and virus strains		
Biological samples		
Critical commercial assays		
RNA-Seq Library Prep kit	Illumina Cat#	Cat# 20020596
RNAScope Multiplex Fluorescent V2 Assay kit	ACD bio	Cat# 323110
Lectin from Wisteria floribunda (WFA)	Sigma	L1516
ATAC-seq Kit	Active Motif	cat#53150
Chemicals, peptides, and recombinant proteins		
RNAscope Probe –Mm-Myrf	ACD bio	Cat# 524061
RNAscope Probe –Mm-Sp7	ACD bio	Cat# 403401
Poly-D-lysine	Sigma-Aldrich	Cat# P6407

REAGENT or RESOURCE	SOURCE	IDENTIFIER
Platelet derived growth factor	PeproTech	Cat# 100-13A
Neurotrophin-3	PeproTech	Cat# 450-03
Ciliary neurotrophic factor	PeproTech	Cat# 450-13
Forskolin	Sigma-Aldrich	Cat# F6886
B27	Life technologies	Cat# 17504044
Fetal bovine serum	Atlanta Biologicals	Cat# S11050
Normal donkey serum	Jackson ImmunoResearch	Cat# 017-000-121
Protease inhibitor cocktail	Thermo Fisher Scientific	Cat# 78430
Phosphatase inhibitors	Sigma-Aldrich	Cat# P2850 and P5726
Laemmli sample buffer	Bio-Rad Laboratories	Cat# 161-0737
β-mercaptoethanol	Sigma-Aldrich	Cat# M6250
Trypsin 0.05%	Thermo Fisher Scientific	Cat# 25300-054
Trypsin 2.5%	Thermo Fisher Scientific	Cat# 15090046
Trypsin inhibitor	Worthington	Cat# LS003086
Deoxyribonuclease I	Worthington	Cat# LS002007
Papain	Worthington	Cat# LS003126
Apo transferrin	Sigma-Aldrich	Cat# T1147
ProLong gold abtifade reagent with DAPI	Life Technologies	Cat# P36931
Paraformadehyde	Thermo Fisher Scientific	Cat# T353-500
Osmium Tetroxide	Electron Microscopy Science	Cat# 19152
Propylene Oxide	Electron Microscopy Science	Cat# 20401
Sodium Cacodylate Buffer	Electron Microscopy Science	Cat# 11652
Epon 812	Electron Microscopy Science	Cat# 14900
Trizol reagent	Thermo Fisher Scientific	Cat# 15596018
Deposited data		
Raw and analyzed data (ChiP-Seq, ATAC-seq and RNA-Seq)	This paper	GSE221193
Sox10 Chip-Seq	He, D et al., [20]	GSE72727
Sp7 ChiP-seq	Wang, JS, et al [29]	GSE154719
Experimental models: Cell lines		
Experimental models: Organisms/strains		
$Sp7^{fl/fl}$ mice [25]	Kindly provided by Dr. Benoit de Crombrugghe	RRID:IMSR_JAX:035391
Olig2-Cre mice[26]	Kindly provided by Dr. William D Richardson	RRID:IMSR_JAX:025567
PLP-CreERt mice [27]	Brian Popko	RRID:IMSR_JAX:005975
PDGFRa-CreERt2 [28]	Kindly provided by Dr. William D Richardson	RRID:MGI:3832569
Oligonucleotides		

REAGENT or RESOURCE	SOURCE	IDENTIFIER
Recombinant DNA		
Software and algorithms		
Image Lab software	Bio-Rad laboratories	RRID: SCR_003070
ImageJ	National Institutes of Health	RRID: SCR_014210
Image Lab	Bio-Rad Laboratories	RRID: SCR_001905
R v3.5.1	R core team	RRID: SCR_002798
GraphPad Prism 6	GraphPad Software	RRID:SCR_018350
HALO software	Indica Labs	RRID: SCR_003070
Other		